microwave

Review

Low-Power Rectennas in Microwave Wireless Power Transmission

Yilin Zhou [1], Ruinan Fan [1] and Changjun Liu [1,2,*]

[1] College of Electronics and Information Engineering, Sichuan University, Chengdu 610064, China; yilin_zhou@stu.scu.edu.cn (Y.Z.); fanruinan@stu.scu.edu.cn (R.F.)
[2] Yibin Industrial Technology Research Institute, Sichuan University, Yibin 644000, China
* Correspondence: cjliu@ieee.org

Abstract: The advancement of microwave wireless power transfer technology has positioned low-power rectennas as a research hotspot. This paper systematically reviews core technological progress in low-power rectennas, focusing on innovations in rectifier circuit topologies, nonlinear device models, antenna array optimization, and efficiency enhancement strategies. Current technical bottlenecks and future application directions are analyzed, providing theoretical references for space solar power stations, IoTs, and related fields.

Keywords: rectenna; rectifier; low-power rectification; Schottky diodes; wireless power transfer (WPT)

check for updates

Academic Editor: Shah Nawaz Burokur

Received: 28 May 2025
Revised: 12 June 2025
Accepted: 13 June 2025
Published: 18 June 2025

Citation: Zhou, Y.; Fan, R.; Liu, C. Low-Power Rectennas in Microwave Wireless Power Transmission. *Microwave* **2025**, *1*, 5. https://doi.org/10.3390/microwave1010005

1. Introduction

Wireless power transfer (WPT) has emerged as a revolutionary technology, enabling the untethered operation of electronic devices across a spectrum of applications, ranging from industrial automation to biomedical implants [1,2]. This technology was initially proposed by Nikola Tesla at the end of the 19th century [3]. Early WPT efforts primarily targeted high-power, short-range transmission using inductive or resonant coupling [4,5]. Recent advancements in microwave engineering have paved the way for efficient far-field energy harvesting [6–8]. In particular, rectennas have garnered increasing attention for their ability to capture and convert low-power-density radio frequency (RF) energy into dc power.

While high-power WPT systems' development is hampered by their bulky size, high implementation, costs and safety concerns arising from elevated radiation levels, low-power-density rectenna systems have found widespread application opportunities as they are uniquely suited to meet the demands of the rapidly expanding Internet of Things (IoT) ecosystem, where vast numbers of distributed sensors and devices require maintenance-free, long-term energy solutions. The proliferation of ambient RF sources, such as cellular base stations, Wi-Fi routers, and broadcasting towers, has created an environment rich in harvestable electromagnetic energy, albeit at relatively low power densities (<100 mW/m^2) [6,9]. This scenario has fueled a surge of innovation focused on maximizing the efficiency and practicality of rectenna designs under real-world operating conditions.

The core challenge in low-power rectenna research lies in optimizing the overall energy conversion process, from the initial RF energy harvesting to efficient rectification into usable dc power. This process must be achieved within the strict constraints of limited available RF power and the need for device miniaturization. Achieving high efficiency in rectenna systems is particularly challenging due to several technical bottlenecks, such as nonlinear losses in rectifying diodes, signal attenuation along transmission lines, and impedance mismatches between antenna and rectifier circuits. Moreover, antenna characteristics, including radiation efficiency, frequency band, polarization orientation, and beam coverage, directly influence the performance of low-power wireless power transmission systems in practical applications.

This review comprehensively overviews recent technological progress in low-power-density rectenna systems. Section 2 discusses key innovations in rectifier circuit design, nonlinear device modeling, and RF-dc efficiency enhancement. Section 3 examines the design requirements of antennas for various application scenarios, highlighting how antenna configurations are optimized to meet diverse operational demands. Section 4 explores the practical applications of low-power rectenna systems in industrial IoT, implantable medical devices, and space solar power stations (SSPSs). Finally, concluding remarks are provided in Section 5.

2. Low-Power Rectifiers

A typical rectenna consists of an antenna and a rectifier, where the antenna serves as the medium for exchanging energy between ambient RF fields and the circuit, and the rectifier is responsible for converting the captured RF energy into dc power. Consequently, the overall efficiency of a rectenna is mainly determined by the rectification efficiency of the rectifier. Schottky barrier diodes are widely adopted in RF rectifier circuit design due to their low forward voltage drop and high switching speed characteristics. Numerous methods have been proposed to obtain closed-form models for diodes. The rectifying diode is ideal for medium to high input power levels. When forward-biased, diode impedance is extremely low and can be approximated by a series resistance Rs, whereas when reverse-biased, its impedance approaches infinity [10,11]. However, the diode's nonlinearity weakens at low input power levels, and the ratio of reverse to forward impedance decreases, making the traditional ON-OFF model no longer applicable [12]. The equivalent circuits corresponding to two states of the Schottky-diode-based rectifier are shown in Figure 1.

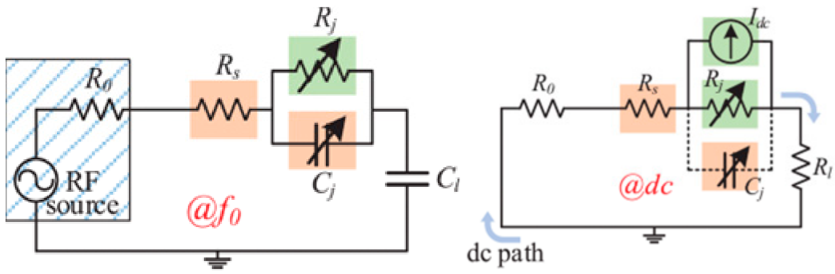

Figure 1. Equivalent circuits corresponding to two states of Schottky-diode-based rectifier: (**a**) RF power absorber, (**b**) dc power provider [12].

In [13], S. Hemour et al. introduced an efficiency chain concept to characterize rectifiers' RF-dc conversion efficiency under low-power conditions. The overall efficiency can be described as the product of four efficiencies:

$$\eta_{RF-dc} = \frac{P_{dc}}{P_{RF}} = \eta_M \cdot \eta_p \cdot \eta_0 \cdot \eta_{DCT}$$

where η_M stands for matching efficiency, representing the reflection loss caused by impedance discontinuity when the signal enters the nonlinear device, as well as additional insertion loss introduced by the matching network; η_p stands for parasitic efficiency, which accounts for the low-pass filtering effect of the diode junction capacitance C_j, causing part of the current reaching the diode to be reflected and consumed by the series resistance. The inherent properties of the diode typically determine the following relationship: the smaller the junction capacitance C_j, junction resistance R_j, and series resistance R_s, the higher the parasitic efficiency. η_0 is the RF-dc conversion efficiency of the diode, mainly governed by the current responsivity $\Re_{I0}$ of the nonlinear junction. A higher current responsivity indicates stronger nonlinearity and thus higher efficiency η_0. The diode fabrication process primarily influences the current responsivity; η_{DCT} stands for dc-load transfer efficiency. The diode can be seen by the load as a dc source with the junction resistance considered the source impedance. The maximum dc-load efficiency η_{DCT} is obtained when the load resistance equals the diode's junction resistance.

It can be seen that under low input power conditions, the energy loss in the rectifier mainly originates from two aspects. One is the loss caused by the diode's intrinsic parameters, primarily due to the weakened nonlinearity at low power levels. The other is the loss in the matching circuits, including impedance discontinuities resulting from imperfect matching network design, additional losses from transmission lines, and dc-load mismatches. It is worth noting that under low input power, the bias voltage V_j of the diode is less than the turn-on voltage V_{bi}, causing the diode to operate in a zero-bias state. In this scenario, most of the energy is dissipated in the junction resistance, while energy loss at higher harmonics is minimal and can therefore be neglected.

2.1. Diode Performance Optimization

Based on the previous discussion of diode efficiency, multiple approaches can be employed to reduce diode losses under low input power conditions.

2.1.1. Input Signal Manipulation

Schottky diodes require a minimum amount of energy to turn on, and the input voltage must exceed a certain threshold to activate the diode and generate a relatively large dc output voltage [14]. Therefore, increasing the input power and voltage delivered to the diode is an effective method to improve efficiency. As shown in Figure 2, a coupled transmission line (CTL) structure was employed to increase the voltage across the diode, thereby enhancing rectifier efficiency. At 2.4 GHz, when the input powers were −5 dBm, 0 dBm, and 5.5 dBm, the rectification efficiencies reached 60.4%, 67.7%, and 75.3%, respectively [15]. Compared to conventional designs, this structure is more effective in reducing losses caused by the built-in potential V_{bi} of the PN junction. Similarly, introducing a high-impedance transmission line before the diode can also increase the input voltage. This approach not only achieves impedance matching between the diode and the source but also boosts the peak diode voltage V_D to four times the input voltage V_{in}. At 5.8 GHz with an input power of −30 dBm, an efficiency of 3.5% was achieved [16].

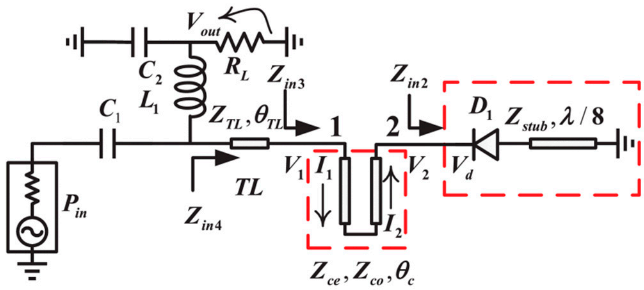

Figure 2. Schematic of CTL-based rectifier [15].

Another method is waveform manipulation. Under the same average input power, the nonlinear combination of multiple sinusoidal signals can better excite the diode, significantly increasing output dc power compared to single-tone excitation [17]. The efficiency improvement from multi-tone signals depends on the diode parameters, with the most significant benefit observed for diodes with high junction capacitance C_j [18]. Several studies have reported that using multi-tone signals increases the rectification efficiency [19–23]. In [24], the multi-tone signal optimization problem was formulated as a linear constrained quadratic program, and a globally optimal solution was proposed based on mixed-integer linear programming and branch-and-bound methods. The diode model was simplified to a second-order polynomial curve-fitting model, providing an excellent solution for multi-tone power allocation strategies. With the rapid development of the Internet of Things (IoT) in recent years, simultaneous wireless information and power transfer (SWIPT) technology have attracted huge attention [25]. Various multi-tone modulation techniques such as BASK [26,27], FSK [28], BFSK [29], and PSK [30,31] have been introduced, enabling simultaneous transmission of energy and information while improving energy conversion efficiency.

Adding other environmental energy sources is the most direct way to increase input power. Green energies such as solar energy [32–35], thermal energy [36–39], and kinetic energy [40–43] can be combined with RF energy to achieve higher dc output power. In [36], a cooperative voltage doubler rectifying topology was proposed, seamlessly integrating RF and photovoltaic energy, as shown in Figure 3. The single-frequency rectifier operating at 2.4 GHz exhibited an ultra-wide input power range from −20 dBm to 5 dBm under a light intensity of 232 Lux, achieving an efficiency of 15% at −20 dBm. The wide-band rectifier employed a post-matching technique, using additional capacitors and transmission lines to compensate for the imaginary part of the diode impedance, achieving efficiencies greater than 30% over the 0.8–2.4 GHz range.

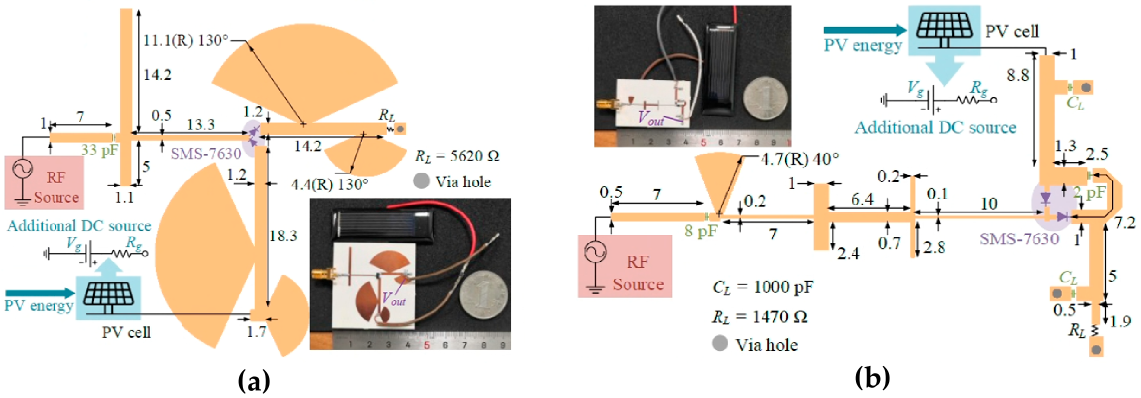

Figure 3. Layout and prototype of: (**a**) single-band, (**b**) wide-band cooperative rectifier [36].

2.1.2. High-Nonlinearity Device Selection

The current responsivity $\Re_{I0}$ of a Schottky diode is defined in the square-law region as the ratio of the output DC current I_0 to the input RF power P_{I0} when the load is shorted [44]. A simpler and general form can be derived from the I-V curve of the diode. $\Re_{I0}$ is an intrinsic property of the diode, limited by its physical mechanisms. The maximum current responsivity attainable by any Schottky diode at ambient temperature is 19.4 A/W. This indicates that the efficiency of current commercial Schottky diodes has reached the theoretical limit, and achieving higher rectification efficiency at low power levels requires exploring devices with stronger nonlinearity.

In 2015, the use of a backward tunnel diode to break the efficiency limitation of Schottky diodes was reported [45]. Compared to conventional Schottky diodes, the backward tunnel diode exhibits a lower parasitic junction capacitance C_j and higher current responsivity $\Re_{I0}$, measured at 4.5 fF and 21.65 A/W, respectively. The photograph of the rectifier can be seen in Figure 4. At 2.4 GHz with an input power of −40 dBm, it achieved a rectification efficiency of 14.6%, which is 13.3 times higher than that of the HSMS-285B and 7 times higher than that of the SMS-7630. The latest ReS_2/BP negative capacitance tunnel field-effect transistor has a response time of 8 µs and a current responsivity of 41 A/W [46]. The metal–insulator–insulator–metal (MI^{2}M) diode, which sandwiches thin insulator layers between two metal electrodes, utilizes the resonant tunneling effect to provide high current responsivity [47,48]. A nanoscale spin rectifier, based on magnetic tunnel junctions, represents a novel type of rectifying device capable of collecting RF energy at extremely low input power levels of −62 dBm. Energy harvesting modules based on arrays of such structures can power commercial sensors at low RF power levels as low as −27 dBm [49]. Table 1 summarizes the key parameters and rectification performance of all the above high-nonlinearity devices.

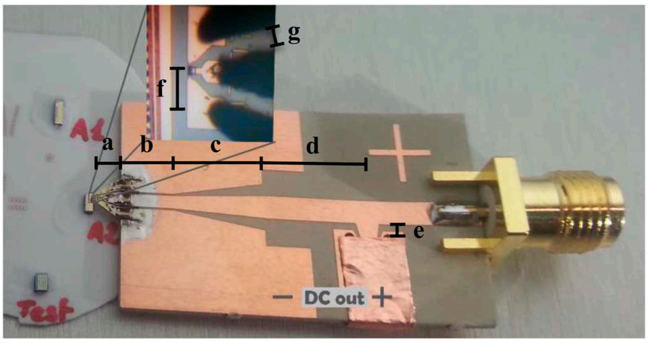

Figure 4. A photograph of the low-power rectifier using a backward diode [45].

Table 1. Key parameters and rectification performance of high-nonlinearity devices.

Ref.	Diode Type	Junction Capacitance	Responsivity	Frequency Band	Rectification Efficiency	Technology Readiness Level
[45]	HSMS-285B	180 fF	18.25 A/W	2.4 GHz	1.1% @ −40 dBm	TRL9
	SMS7630	140 fF	18.42 A/W	2.4 GHz	2.1% @ −40 dBm	TRL9
	Backward Tunnel Diode	4.5 fF	21.65 A/W	2.4 GHz	14.6% @ −40 dBm	TRL8
[46]	NC-TFET	Not Given	41 A/W	Not Given	Not Given *	TRL4
[47]	MI^{2}M	Not Given	36.8 A/W	Not Given	Not Given **	TRL4
[48]	MI^{2}M	Not Given	0.5 A/W @THz Band	28.3 THz	1.7×10^{-8} @ −16.2 dBm	TRL4
[49]	Spin Rectifier	Not Given	10,000 mV/mW @ −62 dBm	2.45 GHz	7.8% @ −27 dBm	TRL4

* The rectification ratio of the device is higher than 10^5 under negative gate voltage, indicating excellent low-power rectifying characteristics. ** The max nonlinearity of the device is 15.8, exhibiting strong rectification characteristics.

2.2. Matching Network Enhancement

The input impedance of the diode is highly sensitive to both input power and frequency at low input power levels. The matching network design becomes critical to ensure the entire input power is delivered to the diode. DC-load matching can also considerably improve efficiency, especially under extremely low-power conditions. However, the matching network itself may introduce additional insertion losses. Therefore, multiple aspects can be addressed to enhance the performance of the matching network.

2.2.1. Robust Matching Network Deployment

With the increasingly widespread application of wireless power transfer (WPT), rectennas' operating frequency band and input power range requirements are becoming more rigorous. The ambient RF energy constantly varies and may come from diverse sources such as FM, 4G cellular, ISM, and the latest 5G NR bands. To harvest more energy, it is essential to broaden the operating bandwidth. However, the input impedance of diodes changes with both input power and frequency, posing significant challenges for matching network design.

Adaptive power allocation technology divides the rectifying circuit into two sub-circuits. It uses either frequency-selective or power-selective networks to separate and route the input signals to dedicated sub-circuits, significantly reducing the difficulty of impedance matching [50–54]. For example, Figure 5 shows a rectifier employing this technology that achieves matching over an input power range from −10 dBm to 30 dBm, and maintains rectification efficiency above 30% from −7 dBm to 30 dBm [50]. A method using low-power varactor diodes to compensate for input impedance dynamically is proposed in [55], as shown in Figure 6. Based on adaptive power allocation, the dc output of one sub-circuit is used as the reverse bias for the varactor diode, enabling self-adaptive capacitance adjustment according to the input power and improving impedance matching without any external bias components. This circuit achieved rectification efficiency above 50% over the input power range of 2.4 dBm to 20.9 dBm. Similar techniques using varactor diodes for improved impedance matching have also been reported in [56,57]. For broadband matching design, multi-stage transmission line matching is a simple and effective approach [58,59]. Impedance compression technology was initially introduced to reduce the variation in the effective resistance of tuned RF inverters under load changes [60]. In recent years, this technique has been widely applied to reduce the sensitivity of diode input impedance, extending the bandwidth and operating power range [61–65]. By employing short-circuited stubs in parallel with transmission lines to form an impedance compression network, the rectifier designed in [65] achieved peak efficiency greater than 70% over the frequency range of 1.0 GHz to 2.7 GHz and the input power range of −6.5 dBm to 13 dBm (Figure 7). A brief comparison of the main features of the impedance matching strategies discussed above is summarized in Table 2. Overall, the multi-stage transmission line matching method exhibits good performance but is unsuitable for low-power scenarios due to its large size and the associated insertion loss. In contrast, the other three approaches simplify circuit complexity and minimize insertion loss. Notably, the varactor-assisted matching method and the impedance compression technique are more suitable for low-power rectifier designs while also achieving a broad input power range and bandwidth.

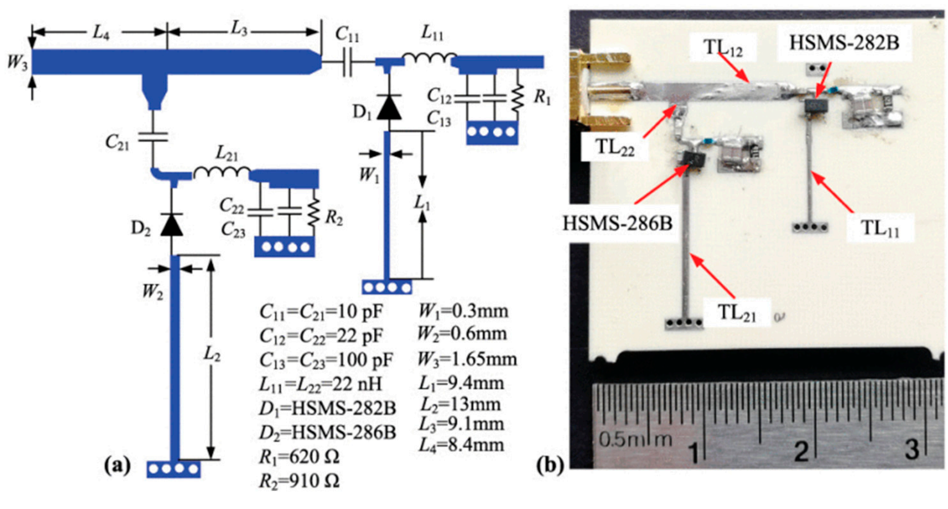

Figure 5. Rectifier with automatic input power distribution technique: (**a**) Layout, (**b**) Photograph of fabricated rectifier [50].

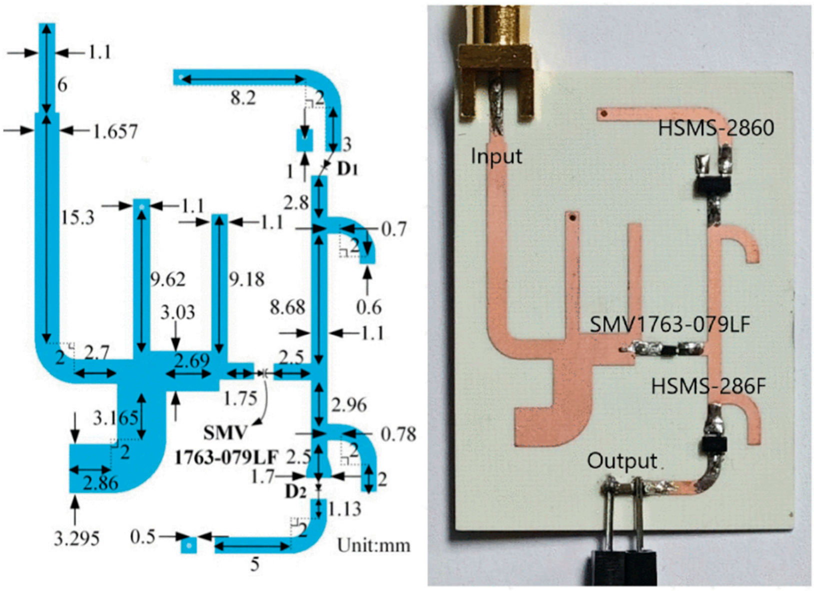

(a) (b)

Figure 6. Wide-power-range rectifier using low-power varactor: (**a**) Layout, (**b**) Photograph of fabricated prototype [55].

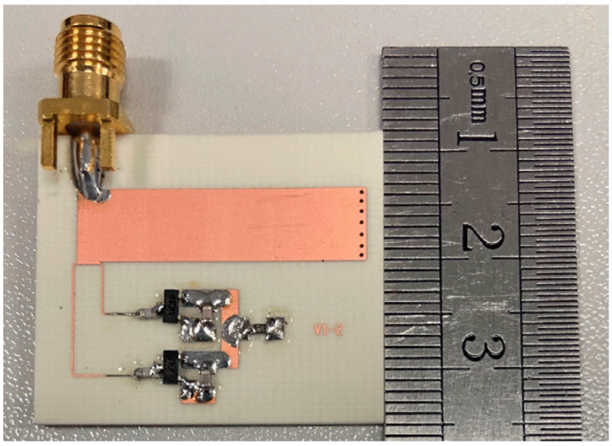

Figure 7. Photograph of ultrawideband rectifier with extended dynamic power range [65].

Table 2. Performance comparison of various impedance matching strategies.

Matching Strategy	Ref.	Power Range	Frequency Range	Insertion Loss	Complexity
Adaptive Power Allocation	[50]	−10 to 30 dBm *	2.4 GHz	Medium	Simple
	[51]	10 dBm	1.7 to 3.6 GHz *		
	[54]	−2 to 18.3 dBm @ 2.45 GHz ** 3 to 19.7 dBm @ 5.8 GHz **	2.45 / 5.8 GHz		
Varactor-Assisted	[55]	2.4 to 20.9 dBm **	2.1 GHz	Low	Moderate
	[56]	2.5 to 25.5 dBm **	2.4 GHz		
	[57]	−21 to −16 dBm **	915 MHz		
Multi-Stage Transmission Line	[58]	10 dBm	2.0 to 3.05 GHz ***	High	Complex
	[59]	10 dBm	450 to 950 MHz ***		
	[61]	5 dBm	1.6 to 2.8 GHz **		
Impedance Compression	[62]	7 to 23 dBm @ 2.35 GHz ** 9 to 21 dBm @ 5.35 GHz **	2.35 / 5.35 GHz	Low	Simplest
	[65]	−5 to 13 dBm @ 1.4GHz **	1.0 to 2.7 GHz @ 6.5dBm **		

* Range for $|S_{11}| < -10$dB. ** Range for efficiency > 50%. *** Range for efficiency > 70%.

2.2.2. Dynamic DC-Load Matching

When the input power is relatively low, the optimal load resistance for a rectifier is generally the sum of the diode's junction resistance R_j and series resistance R_s [14]. To address variations in junction resistance R_j, wide-load techniques are considered to achieve dynamic dc-load matching. Maximum power point tracking (MPPT) technology is widely used for optimal load matching [66–69]. In [67], a fractional open-circuit voltage approximation method was proposed to determine the optimal load. The reconfigurable rectifier designed with this method operates over an input power range from −22 dBm to −2 dBm, maintains an efficiency above 20% from −16 dBm to −2 dBm, and achieves MPPT accuracy exceeding 86%. Reference [68] reported a novel feedback-free fast (f^3) MPPT module based on input power detection and direct parameter adjustment. The block diagram of the controller is shown in Figure 8, which includes an RF power detector, flash ADC, timing controller, REG (register), and logic circuits. The fabricated rectifier, implemented in 0.18 µm CMOS technology, operates over an input power range from −23 dBm to 1 dBm, maintains efficiency above 20% from −17 dBm to 1 dBm, and achieves MPPT accuracy exceeding 96%. Another approach is dynamic self-bias impedance compensation between two sub-rectifiers operating in low-load and high-load regions. The layout of the circuit is shown in Figure 9. Experimental results show that circuits based on this technique achieve efficiency greater than 50% under 0 dBm input power with an output load between 0.4 and 9 kΩ, and can maintain operation over an input power range from −15 dBm to 10 dBm [70].

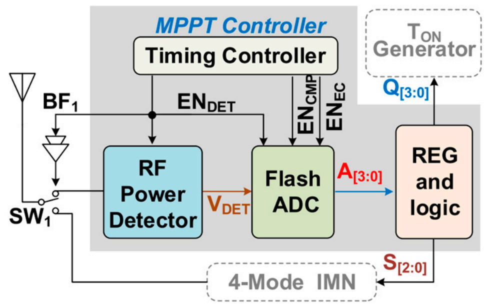

Figure 8. The block diagram of the F3 MPPT controller [68].

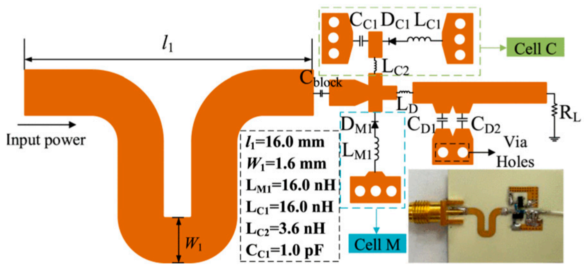

Figure 9. Layout of wide-load-range rectifier based on self-bias impedance compensation [70].

2.2.3. Direct Antenna-to-Rectifier Matching

Conventional rectenna designs typically match the antenna and rectifier output to 50 Ω separately before interconnection. An efficient design approach is to design an inductive antenna to conjugately match the capacitive impedance of the diode, thereby eliminating the matching network [71–74]. In [71], a broadband and high-efficiency rectenna based on this technique is designed, achieving over 60% efficiency within the ranges of 0.9–1.1 GHz and 1.8–2.5 GHz. A novel patch rectenna structure without impedance matching networks is introduced in [73]. The patch antenna is directly connected to the rectifier through a metallic via at the position where the antenna and rectifier's input impedance are conjugately matched, as shown in Figure 10. Ref. [74] proposed an omnidirectional flexible triple-band rectenna for low-power RF energy harvesting without any impedance matching network, which achieved rectification efficiencies of 33.3%, 21.68%, and 15% at 0.915 GHz, 2.45 GHz, and 3.5 GHz, respectively, under an input power of −20 dBm (Figure 11).

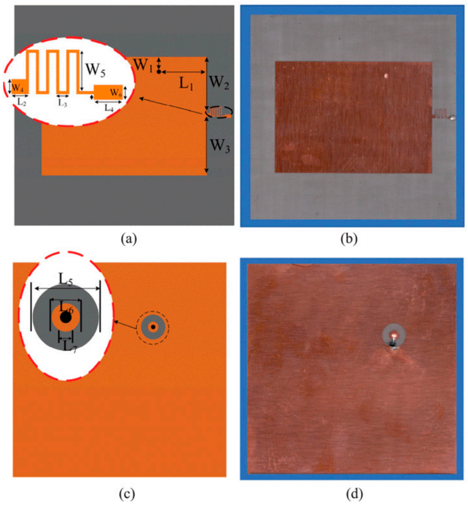

Figure 10. Prototype of single rectifying unit rectenna without matching network: (**a**,**b**) Top views, (**c**,**d**) Bottom views [73].

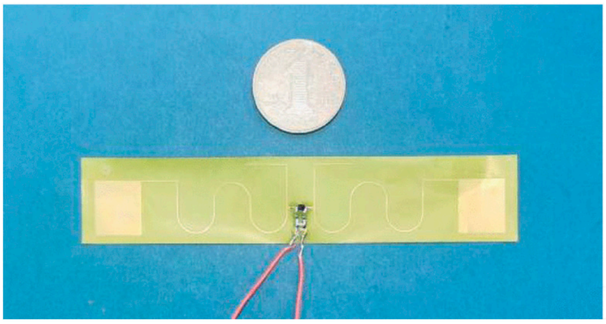

Figure 11. Photograph of tri-band flexible rectenna without impedance matching network [74].

2.2.4. Low-Loss Structure Utilization

Deploying a matching network can significantly reduce reflection losses caused by impedance discontinuities, but it inevitably introduces additional dielectric loss, conductor loss, and radiation loss. Choosing a low-loss dielectric substrate is one way to help improve overall performance [75]. Another way is to use alternative low-loss transmission line structures. The substrate-integrated suspended line (SISL) is a multilayer board structure evolved from the traditional suspended stripline [76]. The upper and lower surfaces of each dielectric layer of the SISL structure are covered with copper, and densely arranged metallized via holes are embedded to form metallic walls, which reduce radiation loss. Additionally, the second and fourth substrate layers are hollowed out to create air cavities for electromagnetic wave propagation, thereby reducing dielectric loss. As shown in Figure 12, a rectifier based on the SISL structure has been demonstrated to operate at extremely low power levels, achieving a rectification efficiency of 3.5% at −30 dBm input power [16]. Due to its ultra-low-loss characteristics, SISL technology has also found widespread application in the millimeter-wave frequency band [77].

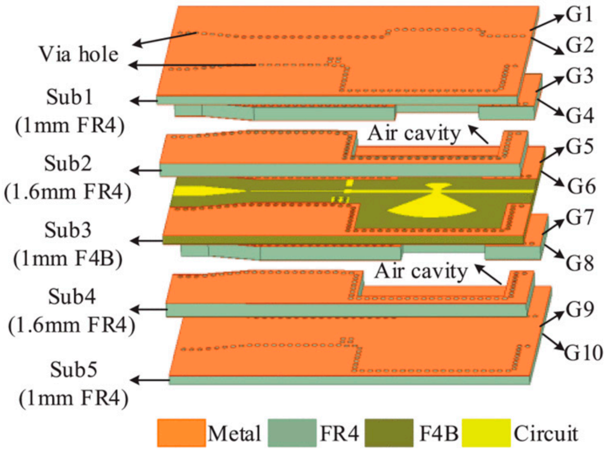

Figure 12. A three-dimensional view of the rectifier based on the SISL platform [16].

3. Low-Power-Density Rectenna

The antenna is a crucial component in a rectenna, harvesting propagating RF energy in free space and providing impedance transformation between free space and the transmission line. Properly designing the receiving antenna can also improve rectification efficiency under low-power-density conditions. Designing high-gain and high-efficiency antennas can increase the power delivered to the rectifier; multiband and wideband antennas can broaden the range of available energy sources; dual-polarized and circularly polarized antennas can capture more polarization components; and multi-beam or beam-steerable antennas can extend the energy harvesting range.

3.1. High-Gain Antenna Design

The theoretical received power P_r at the rectenna can be derived from the Friis transmission equation [78]:

$$P_r = G_t \cdot G_r \cdot \left(\frac{\lambda}{4\pi d}\right)^2 \cdot P_t. \tag{1}$$

The environmental RF energy is typically predetermined in ambient energy harvesting. The higher the gain G_r of the receiving antenna, the greater the power delivered to the rectifier, resulting in higher efficiency. Therefore, designing a high-gain antenna is one of the main approaches to improve rectification efficiency.

The larger the effective aperture of an antenna, the higher its gain; antenna array techniques can be used to obtain greater gain. Figure 13 shows a novel planar substrate-integrated waveguide (SIW)-fed aperture-coupled circularly polarized complementary 4×4 antenna array, achieving a peak gain of 23.4 dBic and a 3 dB gain bandwidth of 22.8% in the millimeter-wave band [79]. A convex optimization formulation for electrically small antenna arrays with reactively loaded parasitic elements is provided in [80]. In this approach, the objective function is to maximize the antenna gain, while the input admittance is used as a constraint to establish a standard convex optimization problem. The conditions for achieving super-gain are analyzed for different array configurations with various combinations of parasitic elements. A millimeter-wave rectenna system based on a Rotman lens was first proposed in 2019, consisting of antennas, rectifiers, a Rotman lens, and a power combining network. Compared to conventional designs, the Rotman rectenna achieved a 21-fold increase in harvested power while maintaining the same angular coverage, thus simultaneously realizing high gain and wide beamwidth [81].

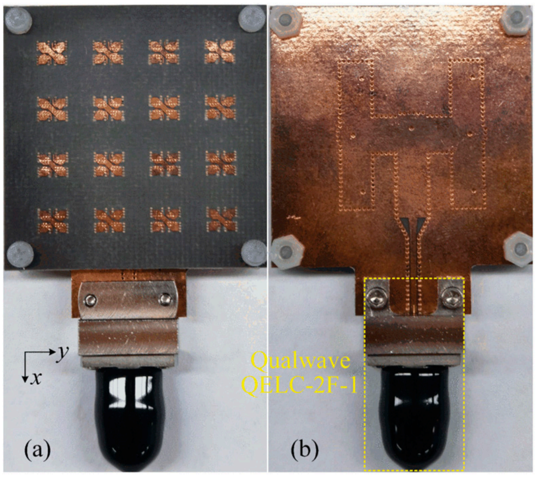

Figure 13. Prototype of 4 × 4 antenna array fed by SIW network: (**a**) Front view, (**b**) Bottom View [79].

3.2. Multi-/Wideband Rectenna Configurations

Ambient RF energy exists across multiple frequency bands; designing multiband or wideband rectennas can help harvest more energy. Reference [82] proposed a triple-band high-gain antenna covering the GSM-1800, UMTS-2100, and Wi-Fi bands. Under an input power of −30 dBm, the rectenna achieves 7.6%, 8.6%, and 4.3% efficiencies at these three bands, respectively. A seven-band rectenna with even broader frequency coverage was first introduced in [83], capable of harvesting RF energy from GSM1800, LTE, Wi-Fi, and various 5G bands. The design process and topology can be seen in Figure 14. This rectenna operates over an ultra-wideband from 1.67 to 5.92 GHz, achieving rectification efficiencies of 49% @ 1.84 GHz, 51% @ 2.04 GHz, 52% @ 2.36 GHz, 53% @ 2.54 GHz, 46% @ 3.3 GHz, 45% @ 4.76 GHz, and 35% @ 5.8 GHz when the input power is around 3 dBm. Furthermore, it can function effectively even under an input power of −20 dBm. In [84], coverage of five commercial frequency bands was achieved using only a single diode, with an average efficiency of 23.2% under −20 dBm input power. Notably, when a five-tone signal was input, an efficiency of 43.7% was attained at −20 dBm input power. Figure 15 introduced a transversely connected folded, tightly coupled ultra-wideband dipole array. By employing capacitive-loaded metallic walls to eliminate the common-mode resonance of the array and broaden the operational bandwidth, the designed 16 × 16 array can operate within the 0.41–3.3 GHz frequency range [85].

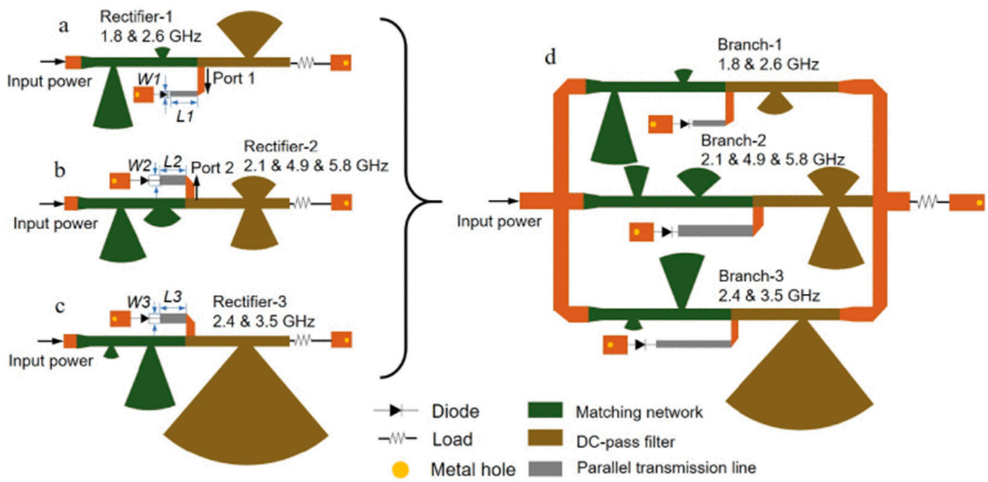

Figure 14. (**a**–**d**) Design process and topology of the seven-band rectenna [83].

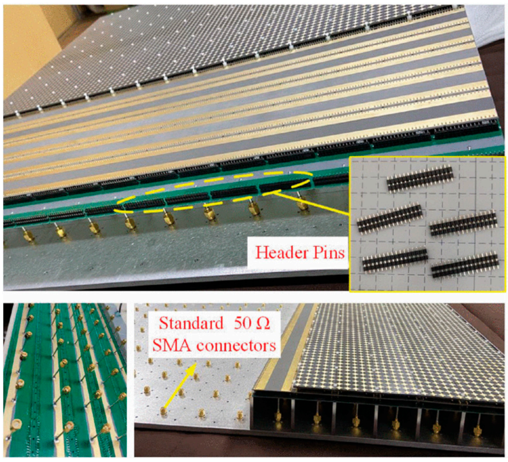

Figure 15. Installation of the fabricated 16 × 16 antenna array [85].

3.3. Multi-Polarization Rectenna Implementations

Polarization mismatch can significantly affect transmission efficiency even if the main lobe directions are aligned. In extreme cases, a vertically polarized antenna cannot receive any power transmitted by a horizontally polarized antenna. Therefore, multi-polarization should be applied to avoid polarization mismatch while ensuring high antenna gain. Circularly polarized antennas can receive radiation without loss from circularly polarized waves with the same rotational direction, in addition to all linearly polarized waves with a 3 dB loss. Thus, circularly polarized antennas are widely used in wireless power transfer (WPT) applications [86]. A novel dual-band circularly polarized antenna for millimeter-wave power transmission (MMPT) was first reported in [87]. As shown in Figure 16, arc-shaped parasitic patches are introduced near the circular patch to form a chiral structure, converting linearly polarized waves into left-handed circularly polarized waves at 24 GHz and right-handed circularly polarized waves at 28 GHz. High gains of 17.1 dBic and 17.0 dBic are achieved at these frequencies, respectively. All-polarization techniques can harvest circular and linearly polarized waves, overcoming polarization mismatch losses [88–90]. In [91], a compact and efficient all-polarization rectenna is introduced. At 2.45 GHz, the rectenna achieves rectification efficiencies exceeding 63% for all polarization angles with a peak efficiency of up to 82.2%.

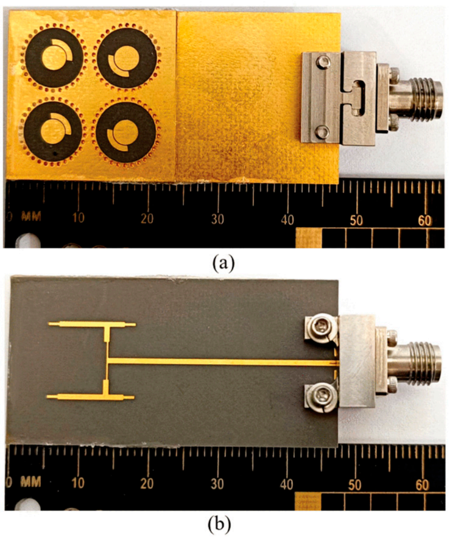

Figure 16. Photographs of the dual-band dual-sense circularly polarized rectenna: (**a**) Front view, (**b**) Bottom View [87].

In order to better compare the performance of various rectennas, Table 3 provides a brief comparison of the main characteristics of several representative rectennas discussed in Sections 3.1–3.3, including parameters such as frequency band, gain, efficiency, and polarization.

Table 3. Performance comparison of different rectenna designs.

Ref.	Operating Frequency (GHz)	Input Power	No. of Elements	Peak Gain	Conversion Efficiency	Polarization State
[79]	33.1–41.6	N/A	4×4	23.4 dBic	N/A	CP
[82]	1.85, 2.15, 2.48	−30 dBm	$2 \times 2 \times 2$	9, 11, 11 dBi	7.6%, 8.6%, 4.3%	Dual-LP
[83]	1.84, 2.04, 2.36, 2.54, 3.3, 4.76, 5.8	3 dBm	1	3 dBi *	49%, 51%, 52%, 53%, 46%, 45%, 35%	N/A
[84]	1.8, 2.1, 2.4, 2.65, 3.5	−20 dBm	2	1.59, 3.18, 2.25, 2.41, 3.46 dBi	21.6%, 26.7%, 28.8%, 19.8%, 17.9%	N/A
[87]	24, 28	18 dBm	2×2	17.1, 17.0 dBic	49.1%, 47.8%	LHCP, RHCP
[89]	1.7–2.5	1 μW/cm^2	1	5 dBi *	24.4%	AP
[91]	2.45	23.3 dBm	1	6.4 dBi	82.2%	AP

CP: circularly polarized. LP: linearly polarized. LHCP: left-hand circularly polarized. RHCP: right-hand circularly polarized. AP: all-polarized. N/A: not available. * Average gain over all operating bands.

3.4. Beamforming Techniques

The beam characteristics of rectennas should be designed according to different application scenarios. Collecting all possible RF energy in the environment is necessary for ambient RF energy harvesting. Therefore, the beam should ideally cover all directions. In contrast, for wireless power transfer targeting dynamic objects, the beam of the rectenna should be steerable to maximize transmission efficiency. Dipole rectennas are widely adopted due to their quasi-full spatial coverage of linearly polarized radiations [92,93]. However, limited by their relatively low gain, dipole rectennas generally exhibit low rectification efficiency. Figure 17 shows a cylindrical flexible antenna array of five vertical antenna arrays, each consisting of four patch antennas. The designed energy harvester can cover 97% of all possible angles of arrival of the incoming radiation. Under an ambient power density of 1 μW/cm^2, a rectification efficiency of up to 45% was achieved [94]. Beamforming networks are the most commonly used method for achieving beam control. Typical beamforming networks include thenRotman lens [95], parabolic reflector [96], Blass matrix [97], Nolen matrix [98], and Butler matrix [99]. Using image recognition technology and beamforming techniques, a 1×4 phased array antenna with target tracking capability was designed, as shown in Figure 18 [100]. Compared with uniform beam transmission, this system can significantly improve transmission efficiency within a distance of approximately ten wavelengths. The time required from target identification to beam phase adjustment is about 100 ms.

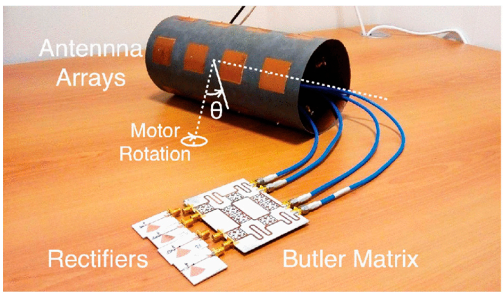

Figure 17. Photograph of cylindrical flexible rectenna [94].

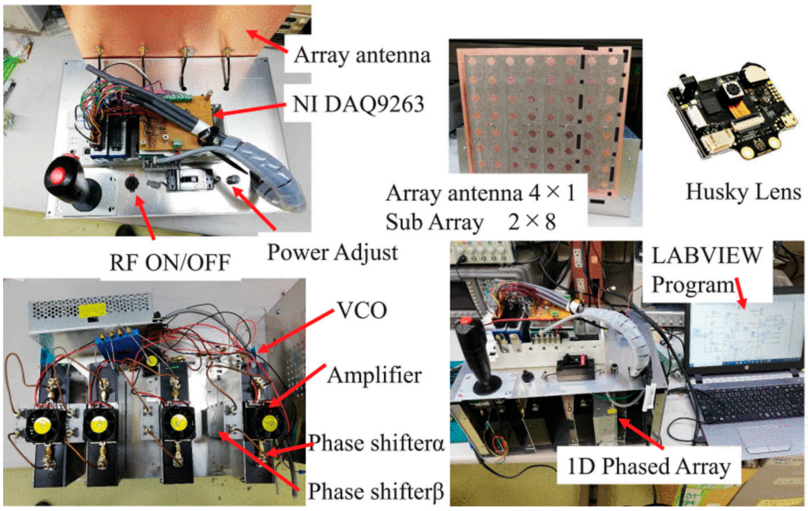

Figure 18. Photograph of tracking phased array [100].

3.5. Advanced Functional Antenna Structures

Conformal antennas are designed to conform to or follow a specific shape, typically mounted on cylinders, cones, hyperboloids, or other complex geometries. By closely adhering to the surface of the supporting platform, conformal antennas offer excellent flexibility and portability and have been widely adopted in both civilian and military applications [101,102]. Figure 19 illustrates a conformal meandered dipole rectenna array designed for Internet of Things (IoT) water meter applications. The antenna elements are wrapped around four faces of the water meter enclosure to enable omnidirectional radio frequency energy harvesting in the environment. When the ambient RF power density reaches 500 $\mu W/cm^2$, the antenna array can deliver a direct current (DC) output power of 7.4 mW [103]. An ultra-wideband implantable conformal antenna for wireless capsule endoscopy is proposed in [104]. Utilizing a bent-line technique, a compact planar antenna is conformed to a cylindrical capsule with a radius of 3 mm, achieving an operating frequency range of 284 MHz to 825 MHz with a maximum gain of −31.5 dBi. To further improve the adaptability of conformal antennas for wireless power transfer in complex electromagnetic environments, a design methodology assisted by deep reinforcement learning (DRL) is introduced in [105]. The overall system consists of a decision module (DRL), a control module (microcontroller unit, MCU), and a radiation module (conformal patch array). By taking the current phase states and gain of the antenna as inputs, the system employs a deep Q-network (DQN) algorithm to determine the phase adjustment actions. The experimental results demonstrate that the measured performance of the array, after DQN training, closely matches the simulated results for various beam directions, greatly simplifying the design, tuning, and deployment of conformal antennas.

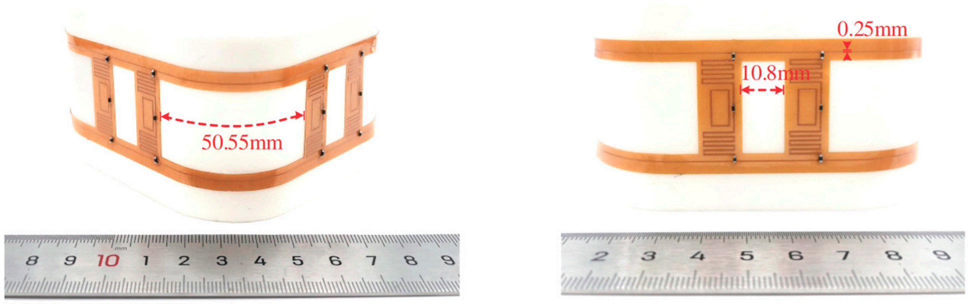

Figure 19. Conformal rectenna array on water meter case [103].

Metamaterials are a novel class of materials engineered with artificially designed and periodically arranged structures, featuring electromagnetic properties beyond those of conventional natural materials. These unique characteristics enable more precise manipulation of light and electromagnetic waves, thereby attracting significant attention from researchers across various fields. By introducing resistive loads into the gaps of metamaterial unit cells, their impedance can be matched to that of free-space wave impedance. This allows metamaterials to function as alternatives to conventional antenna structures for the purpose of wireless energy harvesting (WEH) [106]. Based on such resonator units, various WEH metasurfaces have been proposed, which can achieve high-efficiency RF energy collection under arbitrary polarization angles and across a wide range of incident angles [107–109]. Inspired by rectennas, increasing research efforts have focused on the design of rectifying metasurfaces. Figure 20 presents a two-sided rectifying metasurface for low-power energy harvesting. The front side consists of metasurface units designed based on the electric–inductive–capacitive (ELC) structure, and the backside integrates a voltage-doubling rectifying circuit, separated by a ground plane and interconnected via through-holes. The designed rectifying metasurface achieves an RF-dc conversion efficiency of 76.8% at an input power of 0.4 dBm [110]. To enhance the adaptability of metasurfaces for diverse application scenarios, Engheta et al. proposed the concept of digital metasurfaces, in which two materials with different dielectric constants are encoded as "0" and "1." These coding bits are arranged in mixed patterns to form arrays, enabling flexible modulation characteristics [111]. In the same year, Cui T et al. introduced a similar concept, representing the phase state of surface units as coding bits for metasurfaces, thereby providing a simple, efficient, and flexible control method [112]. Figure 21 illustrates a 2-bit reconfigurable transmissive metasurface array. Each metasurface cell unit comprises a receiver and a transmitter, including loop antennas, DC layers, and ground planes. Each unit embeds four PIN diodes, enabling four different transmission phase states through various combinations, corresponding to 2-bit digital control [113].

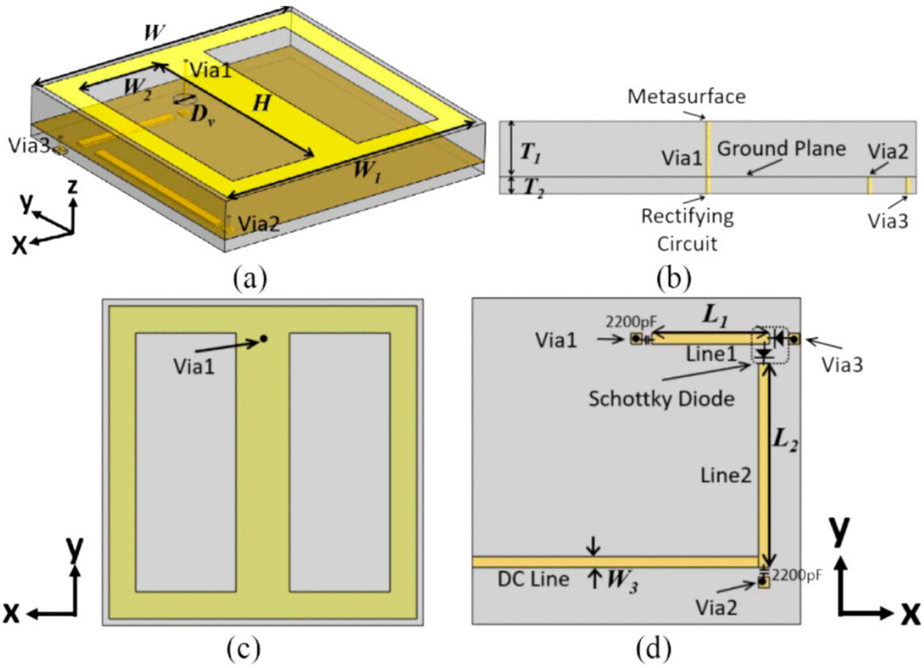

Figure 20. Unit cell of low-power rectifying metasurface: (**a**) Overall view, (**b**) Side view, (**c**) Front view, (**d**) Bottom view [110].

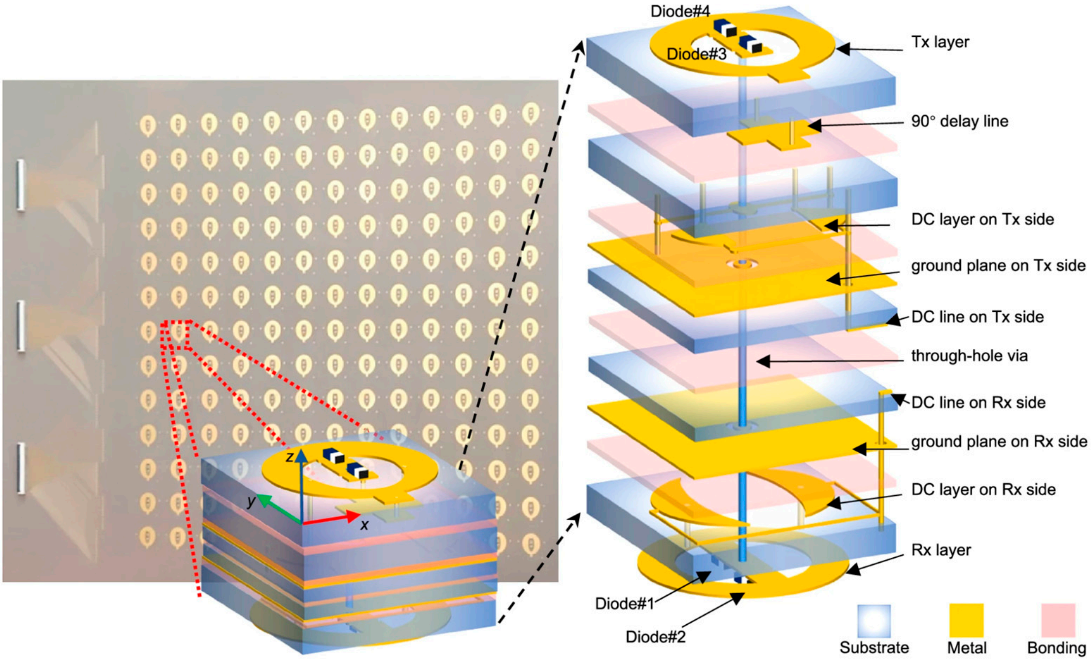

Figure 21. The reconfigurable transmissive metasurface and an exploded view of the unit cell [113].

4. Emerging Application Scenarios

The advancement of wireless power transmission has unlocked new possibilities for battery-free operation in various devices and systems. This WPT technology has benefited from the rapid development of rectennas, capable of harvesting ambient or directional RF energy and converting it into dc power. Depending on the source and strength of the harvested RF signals, wireless power transmission can be categorized into ambient RF energy harvesting and directive RF power transfer. Although ubiquitous and freely available, ambient RF energy is typically exhibited at low and fluctuating power levels, making it particularly suitable for devices with low-power consumption and low-duty-cycle requirements. In contrast, directive RF power transfer can provide higher and more predictable energy levels to support continuous and stable operation in more demanding applications.

The practical integration of energy harvesting rectennas into real-world scenarios has been promoted by the proliferation of low-power electronics and the emergence of ubiquitous wireless communication networks such as Bluetooth Low Energy (BLE) [114–116], RFID [117–119], LoRa [120–122], and ZigBee [123–125]. These networks enable efficient data transmission with minimal energy consumption, which is essential to realizing the vision of sustainable, maintenance-free sensor networks. For example, ambient RF energy harvested from sources like LTE, GSM, or Wi-Fi signals has already been demonstrated to power microcontroller-based sensor nodes in urban environments, achieving significant efficiencies and enabling devices to operate autonomously in active, standby, and low-power modes [126–128]. In addition, integrating energy storage elements such as supercapacitors and batteries with rectenna-based power management modules smooths out intermittent energy supply, supporting long-term and reliable device operation [129,130]. Adaptive energy-aware interfaces between power harvesting modules and sensors further optimize energy transfer based on dynamic load conditions, ensuring maximum power to the required devices even in variable environments [131,132].

The range of applications for low-power rectennas is rapidly expanding across multiple areas. In industrial environments, wireless energy harvesting is driving the development of maintenance-free IoT sensors that enable real-time monitoring and automation in smart manufacturing. Figure 22 shows IoT temperature and light sensors based on two ultrathin electrically small rectennas types. The sensor-augmented rectifier is seamlessly integrated with the antenna and printed on a single ultra-thin PCB. When the ambient temperature increases, the thermistor's resistance decreases, resulting in a rise in the output DC voltage. Once the temperature exceeds 65 °C, the output voltage surpasses 0.8 V, which triggers the acoustic siren. For light detection, the resistance of the photocell is nearly infinite in a dark environment. As the ambient light goes bright, its resistance decreases, causing the output voltage to rapidly rise to 5.9 V and activating the alarm. This design enables a dual-mode detection system for environmental temperature and light intensity [133]. Figure 23 illustrates a novel fully integrated planar six-sector 3D spherical coverage rectenna array designed for wireless energy harvesting applications. Each array sector contains an end-fire element and a bore-sight patch antenna element. The DC output is extracted from the center of the structure via output pins at the bottom, allowing the rectenna array to be directly mounted on IoT nodes for immediate use [134].

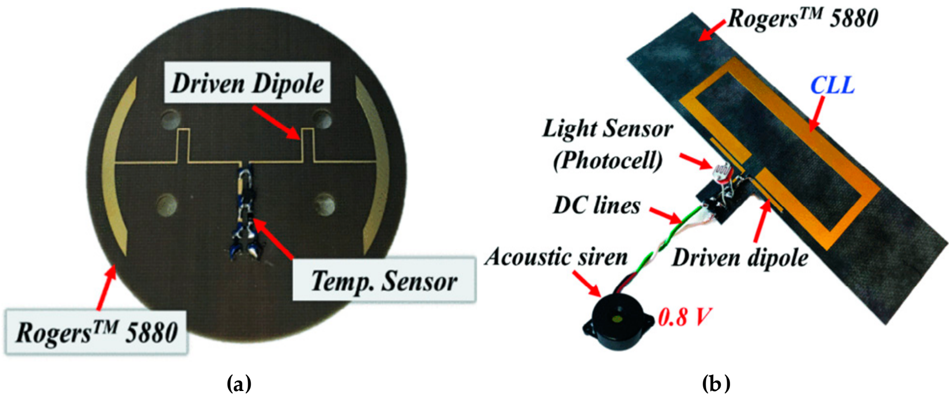

Figure 22. (**a**) IoT temperature sensor, (**b**) IoT light sensor based on ultra-thin Huygens antenna [133].

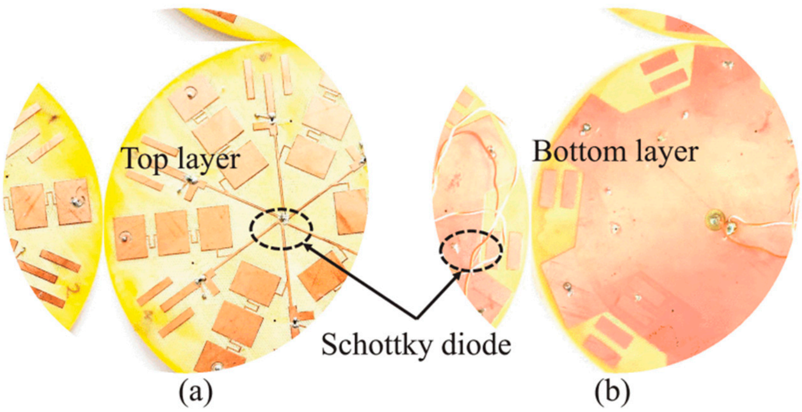

Figure 23. An image of a fabricated planar fully integrated rectenna array for orientation-oblivious energy harvesting: (**a**) Top view, (**b**) Bottom view [134].

In healthcare, implantable medical devices powered by ambient or directive RF energy are emerging as a promising solution for continuous, uninterrupted health monitoring without frequent recharging or battery replacement constraints. Figure 24 presents a flexible and wearable hybrid RF and solar energy harvesting system consisting of a flexible transparent antenna, a flexible transparent rectifier, and an amorphous silicon solar cell. The system can cover the n78/n79 5G communication bands. Under a light intensity of 210 Lux, the system achieves an additional 35.6% to 769.5% output power compared to a single solar cell within an input power range of 4 dBm to 10 dBm [135]. Figure 25 demonstrates wireless power transfer to electronic devices placed in the gastrointestinal (GI) tract using 1.2 GHz mid-field antennas. One antenna is positioned externally, while the other is placed in an anesthetized pig's esophagus, stomach, and colon. The received power levels at these locations are 37.5 µW, 123 µW, and 173 µW, respectively. Wireless powering of medical devices is realized while maintaining radiation exposure below permissible safety standards [136]. Figure 26 depicts a fully wireless implanted asynchronous cardiac pacemaker consisting of a 1.2 GHz implanted electrode antenna, a rectifier, and a pacing circuit. The implanted electrode prototype was tested in vivo in sheep; the RF energy was transmitted from a horn antenna placed 25 cm above the sheep's thorax to the implanted electrode. Asynchronous pacing was successfully achieved while ensuring radiation safety [137].

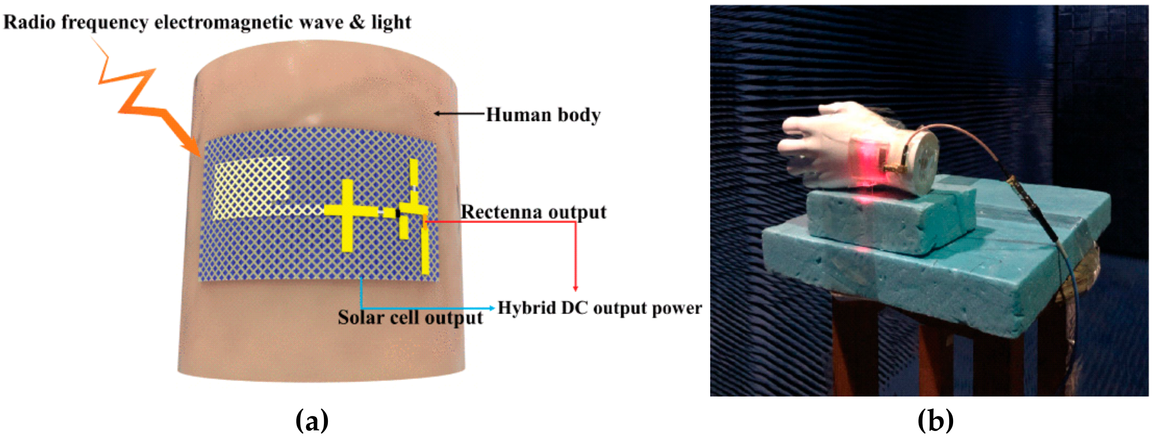

Figure 24. Flexible and wearable hybrid RF–solar energy harvesting system: (**a**) Illustration of system, (**b**) Measurement on human arm model [135].

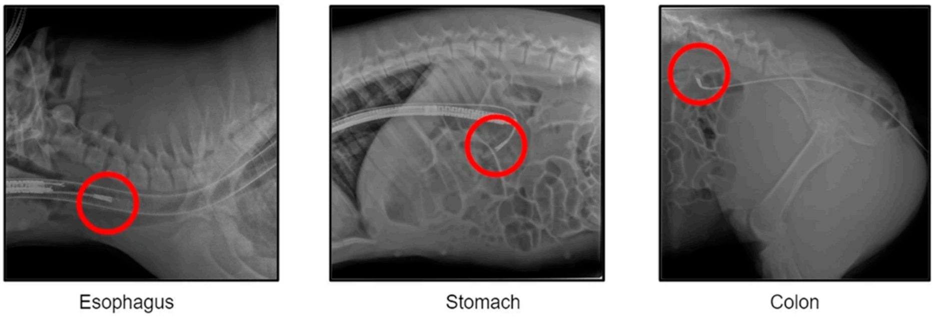

Figure 25. The locations where the 1.2 GHz mid-field antenna is placed [136].

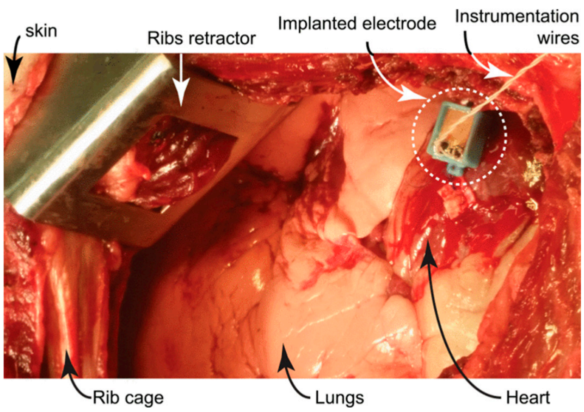

Figure 26. A picture of a fully wireless implanted asynchronous cardiac pacemaker implanted in a sheep's thorax [137].

Furthermore, in the context of renewable energy and space exploration, space solar power stations (SSPSs) have been proposed to collect solar energy in orbit and transmit it wirelessly to Earth via RF beams, representing a visionary application for wireless power transmission [138–140]. According to the development roadmap for the SSPS outlined by the Japan Aerospace Exploration Agency (JAXA), the 100 MW level space demonstration is scheduled for completion by 2030, with commercial operation of gigawatt SSPSs expected before 2040 [141]. In [142], the challenges and solutions for improving the conversion efficiency of rectennas under both low and high input power levels are discussed. The paper also outlines the requirements of rectennas for SSPSs and introduces key technologies for achieving efficient rectification at different input power levels. Figure 27 shows a demonstration system designed to simulate the operational mode of microwave power transmission in a future SSPS. Operating at a frequency of 5.8 GHz, the system achieves a transmission distance of 55 m between the transmitting antenna and the rectenna. The transmitted microwave power is approximately 1600 W, with a DC output power exceeding 300 W. The beam control accuracy is better than 0.4°, which can promote the development of wireless transmission systems for SSPSs [143].

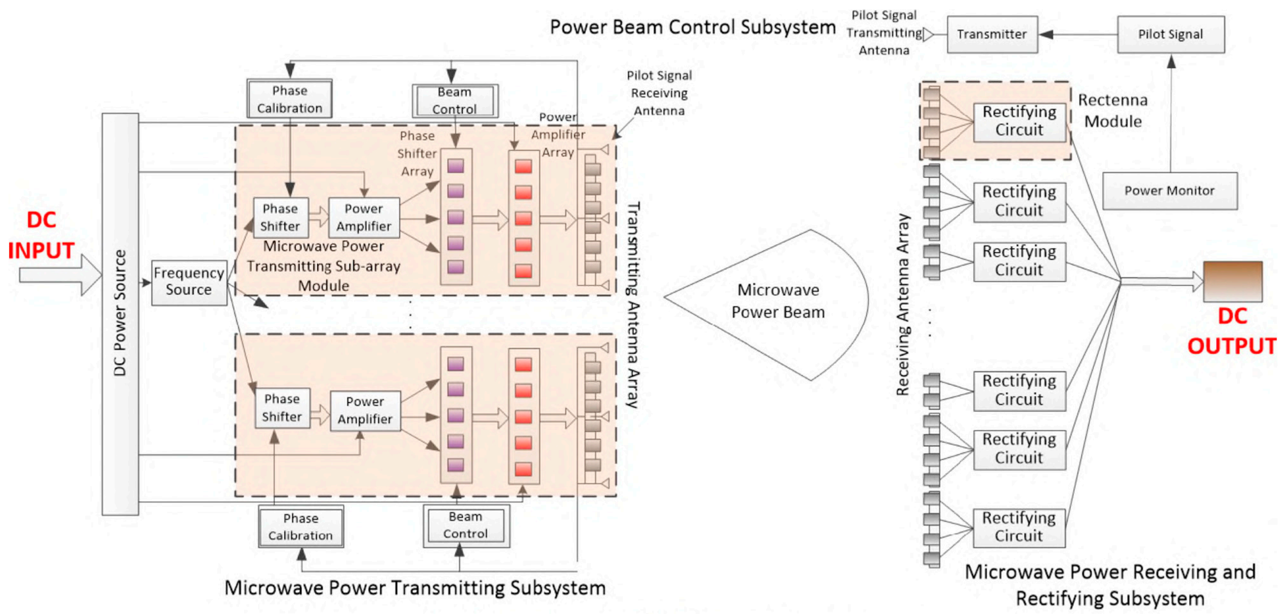

Figure 27. Demonstration of MPT in future SSPS [143].

5. Conclusions

This article discusses technological breakthroughs and industrial applications of low-power-density rectennas in wireless power transmission. As an integrated system, a rectenna primarily consists of a rectifier and an antenna. The rectification efficiency of the rectifier under low input power is mainly limited by the intrinsic properties of nonlinear diodes and additional losses introduced by the matching networks. This review has examined various strategies for improving diode performance and recent innovations in matching networks and transmission line structures. In addition, as the critical interface between the rectifier and ambient RF energy, the antenna should not only achieve high gain but also be capable of multiband/wideband, multi-polarization/omni-polarization, or multi-beam/beam-controllable functionalities according to the application scenarios. Looking ahead, the rapid development of rectenna technology has contributed to both technological progress and industrial innovation, showing great potential to replace batteries or other rechargeable devices. Rectennas are expected to find broad applications in industrial IoT, smart home systems, wearable electronics, implanted healthcare devices, and the realization of future SSPSs.

Funding: This research was funded by NSFC under grant number U22A2015.

Data Availability Statement: Not applicable.

Conflicts of Interest: The authors declare no conflicts of interest.

References

1. Popovic, Z.; Falkenstein, E.A.; Costinett, D.; Zane, R. Low-Power Far-Field Wireless Powering for Wireless Sensors. *Proc. IEEE* **2013**, *101*, 1397–1409. [CrossRef]
2. Khan, A.N.; Cha, Y.-O.; Giddens, H.; Hao, Y. Recent Advances in Organ-Specific Wireless Bioelectronic Devices: Perspective on Biotelemetry and Power Transfer Using Antenna Systems. *Engineering* **2022**, *11*, 27–41. [CrossRef]
3. Tesla, N. The transmission of electric energy without wires. *Electr. World Eng.* **1904**, *1*, 21–24. [CrossRef]
4. Kurs, A.; Karalis, A.; Moffatt, R.; Joannopoulos, J.D.; Fisher, P.; Soljačić, M. Wireless power transfer via strongly coupled magnetic resonances. *Science* **2007**, *317*, 83–86. [CrossRef] [PubMed]
5. Brown, W.C. Free-space transmission. *IEEE Spectr.* **1964**, *1*, 86–91. [CrossRef]
6. Pinuela, M.; Mitcheson, P.D.; Lucyszyn, S. Ambient RF energy harvesting in urban and semi-urban environments. *IEEE Trans. Microw. Theory Tech.* **2013**, *61*, 2715–2726. [CrossRef]
7. Belo, D.; Ribeiro, D.C.; Pinho, P.; Carvalho, N.B. A Selective, Tracking, and Power Adaptive Far-Field Wireless Power Transfer System. *IEEE Trans. Microw. Theory Tech.* **2019**, *67*, 3856–3866. [CrossRef]
8. Shinohara, N. History and innovation of wireless power transfer via microwaves. *IEEE J. Microw.* **2021**, *1*, 218–228. [CrossRef]
9. Kim, S.; Vyas, R.; Bito, J.; Niotaki, K.; Collado, A.; Georgiadis, A.; Tentzeris, M.M. Ambient RF Energy-Harvesting Technologies for Self-Sustainable Standalone Wireless Sensor Platforms. *Proc. IEEE* **2014**, *102*, 1649–1666. [CrossRef]
10. Yoo, T.-W.; Chang, K. Theoretical and experimental development of 10 and 35 GHz rectennas. *IEEE Trans. Microw. Theory Tech.* **1992**, *40*, 1259–1266. [CrossRef]
11. McSpadden, J.; Fan, L.; Chang, K. Design and experiments of a high-conversion-efficiency 5.8-GHz rectenna. *IEEE Trans. Microw. Theory Tech.* **1998**, *46*, 2053–2060. [CrossRef]
12. Gu, X.; Hemour, S.; Wu, K. Far-Field Wireless Power Harvesting: Nonlinear Modeling, Rectenna Design, and Emerging Applications. *Proc. IEEE* **2021**, *110*, 56–73. [CrossRef]
13. Hemour, S.; Zhao, Y.; Lorenz, C.H.P.; Houssameddine, D.; Gui, Y.; Hu, C.-M.; Wu, K. Towards Low-Power High-Efficiency RF and Microwave Energy Harvesting. *IEEE Trans. Microw. Theory Tech.* **2014**, *62*, 965–976. [CrossRef]
14. Lorenz, C.H.P.; Hemour, S.; Wu, K. Physical Mechanism and Theoretical Foundation of Ambient RF Power Harvesting Using Zero-Bias Diodes. *IEEE Trans. Microw. Theory Tech.* **2016**, *64*, 2146–2158. [CrossRef]
15. Zhao, F.; Inserra, D.; Gao, G.; Huang, Y.; Li, J.; Wen, G. High-Efficiency Microwave Rectifier With Coupled Transmission Line for Low-Power Energy Harvesting and Wireless Power Transmission. *IEEE Trans. Microw. Theory Tech.* **2020**, *69*, 916–925. [CrossRef]
16. Liu, D.; Wang, L.; He, Z.; Liu, C. A Self-Packaged SISL Low-Power Rectifier Based on a High-Impedance Line for C-Band Applications. *IEEE Microw. Wirel. Technol. Lett.* **2022**, *33*, 212–215. [CrossRef]
17. Boaventura, A.S.; Carvalho, N.B. Maximizing DC power in energy harvesting circuits using multisine excitation. In Proceedings of the 2011 IEEE MTT-S International Microwave Symposium, Baltimore, MD, USA, 5–10 June 2011; pp. 1–4. [CrossRef]
18. He, Z.; Trovarello, S.; Benassi, F.; Masotti, D.; Liu, C.; Costanzo, A. Analysis of Rectifiers Under Various Multitone Excitations and Using Different Diodes in Low-Power Conditions. In Proceedings of the 2022 IEEE 12th International Conference on RFID Technology and Applications (RFID-TA), Cagliari, Italy, 12–14 September 2022; pp. 157–160. [CrossRef]
19. Boaventura, A.J.S.; Collado, A.; Georgiadis, A.; Carvalho, N.B. Spatial Power Combining of Multi-Sine Signals for Wireless Power Transmission Applications. *IEEE Trans. Microw. Theory Tech.* **2014**, *62*, 1022–1030. [CrossRef]
20. Collado, A.; Georgiadis, A. Optimal Waveforms for Efficient Wireless Power Transmission. *IEEE Microw. Wirel. Compon. Lett.* **2014**, *24*, 354–356. [CrossRef]
21. Valenta, C.R.; Morys, M.M.; Durgin, G.D. Theoretical Energy-Conversion Efficiency for Energy-Harvesting Circuits Under Power-Optimized Waveform Excitation. *IEEE Trans. Microw. Theory Tech.* **2015**, *63*, 1758–1767. [CrossRef]
22. Azarbahram, A.; López, O.L.A.; Latva-Aho, M. Waveform Optimization and Beam Focusing for Near-Field Wireless Power Transfer With Dynamic Metasurface Antennas and Non-Linear Energy Harvesters. *IEEE Trans. Wirel. Commun.* **2025**, *24*, 1031–1045. [CrossRef]
23. Eidaks, J.; Kusnins, R.; Babajans, R.; Cirjulina, D.; Semenjako, J.; Litvinenko, A. Fast and Accurate Approach to RF-DC Conversion Efficiency Estimation for Multi-Tone Signals. *Sensors* **2022**, *22*, 787. [CrossRef]

24. Mouris, B.A.; Ghauch, H.; Thobaben, R.; Jonsson, B.L.G. Multi-Tone Signal Optimization for Wireless Power Transfer in the Presence of Wireless Communication Links. *IEEE Trans. Wirel. Commun.* **2020**, *19*, 3575–3590. [CrossRef]
25. Varshney, L.R. Transporting information and energy simultaneously. In Proceedings of the 2008 IEEE International Symposium on Information Theory, Toronto, ON, Canada, 6–11 July 2008; pp. 1612–1616. [CrossRef]
26. Claessens, S.; Pan, N.; Rajabi, M.; Schreurs, D.; Pollin, S. Enhanced Biased ASK Modulation Performance for SWIPT With AWGN Channel and Dual-Purpose Hardware. *IEEE Trans. Microw. Theory Tech.* **2018**, *66*, 3478–3486. [CrossRef]
27. Debels, E.; Moeneclaey, M. Optimized Linear and Non-Linear Precoding for Biased ASK Modulation in Multiuser SWIPT With Integrated Receiver. *IEEE Trans. Commun.* **2022**, *70*, 6083–6094. [CrossRef]
28. Claessens, S.; Pan, N.; Schreurs, D.; Pollin, S. Multitone FSK Modulation for SWIPT. *IEEE Trans. Microw. Theory Tech.* **2019**, *67*, 1665–1674. [CrossRef]
29. Qaragoez, Y.; Pollin, S.; Schreurs, D. Biased-FSK Modulation for Simultaneous Wireless Information and Power Transfer. *IEEE Trans. Microw. Theory Tech.* **2024**, *72*, 7071–7084. [CrossRef]
30. Dhull, P.; Schreurs, D.; Paolini, G.; Costanzo, A.; Abolhasan, M.; Shariati, N. Multitone PSK Modulation Design for Simultaneous Wireless Information and Power Transfer. *IEEE Trans. Microw. Theory Tech.* **2024**, *72*, 446–460. [CrossRef]
31. Ayir, N.; Riihonen, T.; Heino, M. Practical Waveform-to-Energy Harvesting Model and Transmit Waveform Optimization for RF Wireless Power Transfer Systems. *IEEE Trans. Microw. Theory Tech.* **2023**, *71*, 5498–5514. [CrossRef]
32. Niotaki, K.; Collado, A.; Georgiadis, A.; Kim, S.; Tentzeris, M.M. Solar/Electromagnetic Energy Harvesting and Wireless Power Transmission. *Proc. IEEE* **2014**, *102*, 1712–1722. [CrossRef]
33. Collado, A.; Georgiadis, A. Conformal Hybrid Solar and Electromagnetic (EM) Energy Harvesting Rectenna. *IEEE Trans. Circuits Syst. I Regul. Pap.* **2013**, *60*, 2225–2234. [CrossRef]
34. Zhang, Y.; Shen, S.; Chiu, C.Y.; Murch, R. Hybrid RF-Solar Energy Harvesting Systems Utilizing Transparent Multiport Micromeshed Antennas. *IEEE Trans. Microw. Theory Tech.* **2019**, *67*, 4534–4546. [CrossRef]
35. Shi, Y.; Nan, Y.H. Hybrid Power Harvesting From Ambient Radiofrequency and Solar Energy. *IEEE Antennas Wirel. Propag. Lett.* **2022**, *21*, 2382–2386. [CrossRef]
36. Zeng, B.H.; Zheng, S.Y.; Chan, W.S. Single-and Wide-Band Cooperative Rectifiers Harvesting Ambient Electromagnetic-Photovoltaic Energy for Powering Battery-Less Sensors. *IEEE Internet Things J.* 2025, *early access*. [CrossRef]
37. Guo, L.; Gu, X.; Chu, P.; Hemour, S.; Wu, K. Collaboratively Harvesting Ambient Radiofrequency and Thermal Energy. *IEEE Trans. Ind. Electron.* **2020**, *67*, 3736–3746. [CrossRef]
38. Liu, Z.; Hsu, Y.-P.; Hella, M.M. A Thermal/RF Hybrid Energy Harvesting System With Rectifying-Combination and Improved Fractional-OCV MPPT Method. *IEEE Trans. Circuits Syst. I Regul. Pap.* **2020**, *67*, 3352–3363. [CrossRef]
39. Bakytbekov, A.; Nguyen, T.Q.; Zhang, G.; Strano, M.S.; Salama, K.N.; Shamim, A. Dual-Function Triple-Band Heatsink Antenna for Ambient RF and Thermal Energy Harvesting. *IEEE Open J. Antennas Propag.* **2022**, *3*, 263–273. [CrossRef]
40. Lorenz, C.H.P.; Hemour, S.; Liu, W.; Badel, A.; Formosa, F.; Wu, K. Hybrid Power Harvesting for Increased Power Conversion Efficiency. *IEEE Microw. Wirel. Compon. Lett.* **2015**, *25*, 687–689. [CrossRef]
41. Gu, X.; Hemour, S.; Wu, K. Enabling Far-Field Ambient Energy Harvesting Through Multi-Physical Sources. In Proceedings of the 2018 Asia-Pacific Microwave Conference (APMC), Kyoto, Japan, 6–9 November 2018; pp. 204–206. [CrossRef]
42. Nguyen, S.; Amirtharajah, R. A hybrid RF and vibration energy harvester for wearable devices. In Proceedings of the 2018 IEEE Applied Power Electronics Conference and Exposition (APEC), San Antonio, TX, USA, 4–8 March 2018; pp. 1060–1064. [CrossRef]
43. Xiong, J.; Xia, Y.; Chen, Z.; Xia, H.; Xiao, C. Self-Powered Multiinput Hybrid Rectifier With Arbitrary Phase Difference and Low Start-Up Voltage for Piezoelectric Energy Harvesting. *IEEE Trans. Power Electron.* **2025**, *40*, 4461–4472. [CrossRef]
44. Torrey, H.C.; Whitmer, C.A.; Goudsmit, S.A. *Crystal Rectifiers*; McGraw-Hill: New York, NY, USA, 1948.
45. Lorenz, C.H.P.; Hemour, S.; Li, W.; Xie, Y.; Gauthier, J.; Fay, P.; Wu, K. Breaking the Efficiency Barrier for Ambient Microwave Power Harvesting With Heterojunction Backward Tunnel Diodes. *IEEE Trans. Microw. Theory Tech.* **2015**, *63*, 4544–4555. [CrossRef]
46. Yan, H.; Wu, S.; Chen, Y.; Xiao, Y.; Xiong, K.; Zhao, Q.; Tang, M.; Jiao, H.; Lin, T.; Shen, H.; et al. Negative capacitance tunneling field-effect transistor for logic electronics and photodetection devices. *Appl. Mater. Today* **2025**, *44*, 102737. [CrossRef]
47. Alshehri, A.H.; Shahin, A.; Mistry, K.; Ibrahim, K.H.; Yavuz, M.; Musselman, K.P. Metal-Insulator-Insulator-Metal Diodes with Responsivities Greater Than 30 A W^{-1} Based on Nitrogen-Doped TiO_x and AlO_x Insulator Layers. *Adv. Electron. Mater.* **2021**, *7*, 2100467. [CrossRef]
48. Belkadi, A.; Weerakkody, A.; Moddel, G. Demonstration of resonant tunneling effects in metal-double-insulator-metal (MI^2M) diodes. *Nat. Commun.* **2021**, *12*, 2925. [CrossRef] [PubMed]
49. Sharma, R.; Ngo, T.; Raimondo, E.; Giordano, A.; Igarashi, J.; Jinnai, B.; Zhao, S.; Lei, J.; Guo, Y.-X.; Finocchio, G.; et al. Nanoscale spin rectifiers for harvesting ambient radiofrequency energy. *Nat. Electron.* **2024**, *7*, 653–661. [CrossRef]
50. Wu, P.; Chen, Y.-D.; Zhou, W.; Ren, Z.H.; Huang, S.Y. A Wide Dynamic Range Rectifier Array Based on Automatic Input Power Distribution Technique. *IEEE Microw. Wirel. Compon. Lett.* **2020**, *30*, 437–440. [CrossRef]

51. Wu, P.; Huang, S.Y.; Zhou, W.; Liu, C. One Octave Bandwidth Rectifier With a Frequency Selective Diode Array. *IEEE Microw. Wirel. Compon. Lett.* **2018**, *28*, 1008–1010. [CrossRef]
52. He, Z.; Yan, L.; Liu, C. An Adaptive Power Division Strategy for Nonlinear Components in Rectification. *IEEE Trans. Power Electron.* **2024**, *39*, 15436–15440. [CrossRef]
53. He, Z.; Lan, J.; Liu, C. Compact Rectifiers With Ultra-wide Input Power Range Based on Nonlinear Impedance Characteristics of Schottky Diodes. *IEEE Trans. Power Electron.* **2021**, *36*, 7407–7411. [CrossRef]
54. He, H.; Liao, C.; He, Z.; Yan, L.; Liu, C. An Arbitrary-Frequency Dual-Band High-Efficiency Rectifier Employing a Novel Frequency-Selective Power Allocation Network. *IEEE Trans. Power Electron.* **2025**, *40*, 8939–8943. [CrossRef]
55. Guo, L.; Yan, M.; Li, X.; Guan, K.; Chu, P.; Zhao, Y.; Wu, K. RF Power Harvester With Varactor-Enabled Wide-Power-Range Capability for Wireless Power Transfer Applications. *IEEE Trans. Microw. Theory Tech.* **2025**, *73*, 1848–1856. [CrossRef]
56. Wu, P.; Huang, S.Y.; Zhou, W.; Ren, Z.H.; Liu, Z.; Huang, K.; Liu, C. High-Efficient Rectifier With Extended Input Power Range Based on Self-Tuning Impedance Matching. *IEEE Microw. Wirel. Compon. Lett.* **2018**, *28*, 1116–1118. [CrossRef]
57. De-Oliveira, T.C.; Girardi, A.G.; de Aguirre, P.C.C.; Compassi-Severo, L. A 915-MHz RF-EH with Varactor-Based Adaptive Impedance Matching for ULV Batteryless Devices. In Proceedings of the 2023 Argentine Conference on Electronics (CAE), Cordoba, Argentina, 9–10 March 2023; pp. 112–116. [CrossRef]
58. Wu, P.; Huang, S.Y.; Zhou, W.; Yu, W.; Liu, Z.; Chen, X.; Liu, C. Compact High-Efficiency Broadband Rectifier With Multi-Stage-Transmission-Line Matching. *IEEE Trans. Circuits Syst. II Express Briefs* **2019**, *66*, 1316–13209. [CrossRef]
59. Kimionis, J.; Collado, A.; Tentzeris, M.M.; Georgiadis, A. Octave and Decade Printed UWB Rectifiers Based on Nonuniform Transmission Lines for Energy Harvesting. *IEEE Trans. Microw. Theory Tech.* **2017**, *65*, 4326–4334. [CrossRef]
60. Han, Y.; Leitermann, O.; Jackson, D.A.; Rivas, J.M.; Perreault, D.J. Resistance Compression Networks for Radio-Frequency Power Conversion. *IEEE Trans. Power Electron.* **2007**, *22*, 41–53. [CrossRef]
61. He, H.; Lin, H.; Wu, P.; Li, Q.; Liu, C. Compact High-Efficiency Broadband Rectifier Based on Coupled Transmission Line. *IEEE Trans. Circuits Syst. II Express Briefs* **2022**, *69*, 4404–4408. [CrossRef]
62. Cao, B.; Wu, C.; Zhai, H.; Xu, K.; Chen, Z.; Zhou, R.; Yang, T.; Cai, X.; Li, G. A Dual-Band Rectifier With a Novel Impedance Compression Network for WPT. *IEEE Trans. Power Electron.* **2025**, *40*, 7646–7650. [CrossRef]
63. Song, C.; Huang, Y.; Zhou, J.; Carter, P. Improved Ultrawideband Rectennas Using Hybrid Resistance Compression Technique. *IEEE Trans. Antennas Propag.* **2017**, *65*, 2057–2062. [CrossRef]
64. He, Z.; Liu, C. A Compact High-Efficiency Broadband Rectifier With a Wide Dynamic Range of Input Power for Energy Harvesting. *IEEE Microw. Wirel. Compon. Lett.* **2020**, *30*, 433–436. [CrossRef]
65. Bo, S.F.; Ou, J.-H.; Zhang, X.Y. Ultrawideband Rectifier With Extended Dynamic-Power-Range Based on Wideband Impedance Compression Network. *IEEE Trans. Microw. Theory Tech.* **2022**, *70*, 4026–4035. [CrossRef]
66. Ling, Y.-X.; Tsai, T.-H. A 6.78MHz Wireless Power Transfer System with Maximum Power Tracking over Wide Load Range. In Proceedings of the 2021 International Symposium on VLSI Design, Automation and Test (VLSI-DAT), Hsinchu, Taiwan, 19–22 April 2021; pp. 1–4. [CrossRef]
67. Zeng, Z.; Estrada-Lopez, J.J.; Abouzied, M.A.; Sanchez-Sinencio, E. A Reconfigurable Rectifier With Optimal Loading Point Determination for RF Energy Harvesting From −22 dBm to −2 dBm. *IEEE Trans. Circuits Syst. II Express Briefs* **2020**, *67*, 87–91. [CrossRef]
68. Liao, X.; Zhang, Y.; Zhang, Y.; Zhang, S.; Zhu, Z.; Liu, L. A High-Efficiency RFEH System With Feedback-Free Fast (F3) MPPT Over a Wide Input Range. *IEEE Trans. Circuits Syst. I Regul. Pap.* **2025**, *72*, 2592–2602. [CrossRef]
69. Guo, L.; Yan, M.; Hu, R.; Du, R.; Chu, P.; Li, Y.; Zhao, Y.; Wu, K. Low RF Power Harvesting Enabled Wireless Sensor Node With Long-Distance Communication Capability. *IEEE Trans. Microw. Theory Tech.* **2025**. *early access*. [CrossRef]
70. Wu, P.; Li, Y.; Chen, Y.-D.; Yu, P.-Y.; Cheng, Y.; Liu, C. Compact Rectifier With Wide Range of Output Load Based on Self-Bias Impedance Compensation. *IEEE Trans. Power Electron.* **2025**, *40*, 4706–4710. [CrossRef]
71. Song, C.; Huang, Y.; Zhou, J.; Carter, P.; Yuan, S.; Xu, Q.; Fei, Z. Matching Network Elimination in Broadband Rectennas for High-Efficiency Wireless Power Transfer and Energy Harvesting. *IEEE Trans. Ind. Electron.* **2017**, *64*, 3950–3961. [CrossRef]
72. Fan, R.; Mi, J.; Liu, C. Terrestrial transparent green energy receiving system designed for Space Solar Power Station. *Space Sol. Power Wirel. Transm.* **2024**, *1*, 102–107. [CrossRef]
73. Liu, C.; Lin, H.; He, Z.; Chen, Z. Compact Patch Rectennas Without Impedance Matching Network for Wireless Power Transmission. *IEEE Trans. Microw. Theory Tech.* **2022**, *70*, 2882–2890. [CrossRef]
74. Du, C.-H.; Cheng, F.; Yang, Y.; Zhu, H.; Gu, C. Omnidirectional Flexible Tri-Band Rectenna With Eliminated Matching Circuit for Ambient RF Energy Harvesting. *IEEE Trans. Microw. Theory Tech.* **2025**, *73*, 674–686. [CrossRef]
75. Chen, Y.-S.; Chiu, C.-W. Maximum Achievable Power Conversion Efficiency Obtained Through an Optimized Rectenna Structure for RF Energy Harvesting. *IEEE Trans. Antennas Propag.* **2017**, *65*, 2305–2317. [CrossRef]
76. Ma, K.; Chan, K.T. Quasi-Planar Circuits with Air Cavities. PCT Patent WO/2007/149046 (USA); US Patent Appln No: 61/405,244, US Patent Number: 13/880, 19 April 2013.

77. Zhang, H.; Li, D.; Wang, Z.; Liu, Y.; Shinohara, N. A High-Efficiency mmWave Rectifier Based on Substrate-Integrated Suspended Lines. *IEEE Microw. Wirel. Technol. Lett.* 2025, *early access*. [CrossRef]
78. Pozar, D.M. *Microwave Engineering*, 4th ed.; University of Massachusetts at Amherst, John Wiley & Sons, Inc.: Amherst, NY, USA, 2012.
79. Sang, J.; Qian, L.; Li, M.; Wang, J.; Zhu, Z. A Wideband and High-Gain Circularly Polarized Antenna Array for Radio-Frequency Energy Harvesting Applications. *IEEE Trans. Antennas Propag.* **2023**, *71*, 4874–4887. [CrossRef]
80. Georgiadis, A.; Carvalho, N.B. A Convex Optimization Approach for the Design of Supergain Electrically Small Antenna and Rectenna Arrays Comprising Parasitic Reactively Loaded Elements. *IEEE Trans. Antennas Propag.* **2022**, *70*, 4674–4682. [CrossRef]
81. Eid, A.; Hester, J.; Tentzeris, M.M. A Scalable High-Gain and Large-Beamwidth mm-wave Harvesting Approach for 5G-powered IoT. In Proceedings of the 2019 IEEE MTT-S International Microwave Symposium (IMS), Boston, MA, USA, 2–7 June 2019; pp. 1309–1312. [CrossRef]
82. Shen, S.; Zhang, Y.; Chiu, C.-Y.; Murch, R. A Triple-Band High-Gain Multibeam Ambient RF Energy Harvesting System Utilizing Hybrid Combining. *IEEE Trans. Ind. Electron.* **2020**, *67*, 9215–9226. [CrossRef]
83. Wang, Y.; Zhang, J.; Su, Y.; Jiang, X.; Zhang, C.; Wang, L.; Cheng, Q. Efficiency Enhanced Seven-Band Omnidirectional Rectenna for RF Energy Harvesting. *IEEE Trans. Antennas Propag.* **2022**, *70*, 8473–8484. [CrossRef]
84. Li, Z.; Zhang, J.-W.; Wang, Y.-C.; He, D.-P.; Zhang, C. Two-Port Five-Band Rectenna for Ultralow Ambient RF Energy Harvesting. *IEEE Antennas Wirel. Propag. Lett.* **2023**, *22*, 1972–1976. [CrossRef]
85. Sun, D.-M.; Hao, Z.-C.; Ding, C.-Y.; Liu, R.-J.; Guo, Z.-J.; Yin, H.-Y. A Low-Profile Ultra-Wideband and Wide-Scanning Phased Array for UHF Applications. *IEEE Trans. Antennas Propag.* **2023**, *71*, 473–486. [CrossRef]
86. Wagih, M.; Weddell, A.S.; Beeby, S. Rectennas for Radio-Frequency Energy Harvesting and Wireless Power Transfer: A Review of Antenna Design [Antenna Applications Corner]. *IEEE Antennas Propag. Mag.* **2020**, *62*, 95–107. [CrossRef]
87. Wang, Y.; Pan, H.; Chan, T.-T. A Dual-Band Dual-Sense Circularly Polarized Rectenna for Millimeter-Wave Power Transmission. *IEEE Trans. Antennas Propag.* **2025**, *73*, 96–107. [CrossRef]
88. Chou, J.-H.; Lin, D.-B.; Weng, K.-L.; Li, H.-J. All Polarization Receiving Rectenna With Harmonic Rejection Property for Wireless Power Transmission. *IEEE Trans. Antennas Propag.* **2014**, *62*, 5242–5249. [CrossRef]
89. Bo, S.F.; Ou, J.-H.; Dong, Y.; Dong, S.-W.; Zhang, X.Y. All-Polarized Wideband Rectenna With Enhanced Efficiency Within Wide Input Power and Load Ranges. *IEEE Trans. Ind. Electron.* **2022**, *69*, 7470–7480. [CrossRef]
90. Wang, S.; Chang, H.-Y. A 3D Rectenna with All-polarization and Omnidirectional Capacity for IoT Applications. In Proceedings of the 2020 IEEE/MTT-S International Microwave Symposium (IMS), Los Angeles, CA, USA, 4–6 August 2020; pp. 1188–1190. [CrossRef]
91. He, H.; Dan, Z.; He, Z.; Liu, C. Compact High-Efficiency All-Polarization Rectenna for Wireless Power Transmission. *IEEE Antennas Wirel. Propag. Lett.* **2025**, *24*, 706–710. [CrossRef]
92. Zeng, M.; Andrenko, A.S.; Liu, X.; Li, Z.; Tan, H.-Z. A Compact Fractal Loop Rectenna for RF Energy Harvesting. *IEEE Antennas Wirel. Propag. Lett.* **2017**, *16*, 2424–2427. [CrossRef]
93. Suh, Y.-H.; Chang, K. A high-efficiency dual-frequency rectenna for 2.45- and 5.8-GHz wireless power transmission. *IEEE Trans. Microw. Theory Tech.* **2002**, *50*, 1784–1789. [CrossRef]
94. Vandelle, E.; Bui, D.H.N.; Vuong, T.-P.; Ardila, G.; Wu, K.; Hemour, S. Harvesting Ambient RF Energy Efficiently With Optimal Angular Coverage. *IEEE Trans. Antennas Propag.* **2019**, *67*, 1862–1873. [CrossRef]
95. Rotman, W.; Turner, R. Wide-angle microwave lens for line source applications. *IEEE Trans. Antennas Propag.* **1963**, *11*, 623–632. [CrossRef]
96. Cheng, Y.J.; Hong, W.; Wu, K. Millimeter-Wave Substrate Integrated Waveguide Multibeam Antenna Based on the bea Principle. *IEEE Trans. Antennas Propag.* **2008**, *56*, 3055–3058. [CrossRef]
97. Blass, J. Multidirectional antenna—A new approach to stacked beams. In *1958 IRE International Convention Record*; IEEE: New York, NY, USA, 1960; pp. 48–50. [CrossRef]
98. Nolen, J. Synthesis of Multiple Beam Networks for Arbitrary Illuminations. Ph.D. Dissertation, Radio Division, Bendix Corp., Baltimore, MD, USA, 1965.
99. Butler, J.; Lowe, R. Beam forming matrix simplifies design of electronically scanned antennas. *Electron. Des.* **1961**, *9*, 170–173.
100. Yang, B.; Mitani, T.; Shinohara, N. Auto-Tracking Wireless Power Transfer System With Focused-Beam Phased Array. *IEEE Trans. Microw. Theory Tech.* **2023**, *71*, 2299–2306. [CrossRef]
101. Zhu, H.; Liang, X.; Ye, S.; Ronghong, J.; Geng, J. A Cylindrically Conformal Array With Enhanced Axial Radiation. *IEEE Antennas Wirel. Propag. Lett.* **2016**, *15*, 1653–1656. [CrossRef]
102. Sanford, G. Conformal microstrip phased array for aircraft tests with ATS-6. *IEEE Trans. Antennas Propag.* **1978**, *26*, 642–646. [CrossRef]
103. Fan, R.; Mi, J.; Jing, J.; Yan, L.; Liu, C. Conformal Flexible Omnidirectional Rectenna Array Designed for Application in IoT Smart Water Meters. *Prog. Electromagn. Res. C* **2024**, *139*, 159–166. [CrossRef]

104. Wang, J.; Leach, M.; Lim, E.G.; Wang, Z.; Pei, R.; Huang, Y. An Implantable and Conformal Antenna for Wireless Capsule Endoscopy. *IEEE Antennas Wirel. Propag. Lett.* **2018**, *17*, 1153–1157. [CrossRef]
105. Zhang, B.; Jin, C.; Cao, K.; Lv, Q.; Mittra, R. Cognitive Conformal Antenna Array Exploiting Deep Reinforcement Learning Method. *IEEE Trans. Antennas Propag.* **2022**, *70*, 5094–5104. [CrossRef]
106. AlShareef, M.R.; Ramahi, O.M. Electrically small particles combining even- and odd-mode currents for microwave energy harvesting. *Appl. Phys. Lett.* **2014**, *104*, 253906. [CrossRef]
107. Zhang, X.; Liu, H.; Li, L. Tri-band miniaturized wide-angle and polarization-insensitive metasurface for ambient energy harvesting. *Appl. Phys. Lett.* **2017**, *111*, 071902. [CrossRef]
108. Karakaya, E.; Bagci, F.; Yilmaz, A.E.; Akaoglu, B. Metamaterial-Based Four-Band Electromagnetic Energy Harvesting at Commonly Used GSM and Wi-Fi Frequencies. *J. Electron. Mater.* **2019**, *48*, 2307–2316. [CrossRef]
109. Yu, F.; Yang, X.; Zhong, H.; Chu, C.; Gao, S. Polarization-insensitive wide-angle-reception metasurface with simplified structure for harvesting electromagnetic energy. *Appl. Phys. Lett.* **2018**, *113*, 123903. [CrossRef]
110. Lee, K.; Hong, S.K. Rectifying Metasurface With High Efficiency at Low Power for 2.45 GHz Band. *IEEE Antennas Wirel. Propag. Lett.* **2020**, *19*, 2216–2220. [CrossRef]
111. Della Giovampaola, C.; Engheta, N. Digital metamaterials. *Nat. Mater.* **2014**, *13*, 1115–1121. [CrossRef]
112. Cui, T.J.; Qi, M.Q.; Wan, X.; Zhao, J.; Cheng, Q. Coding metamaterials, digital metamaterials and programmable metamaterials. *Light Sci. Appl.* **2014**, *3*, e218. [CrossRef]
113. Li, W.; Yu, Q.; Qiu, J.H.; Qi, J. Intelligent wireless power transfer via a 2-bit compact reconfigurable transmissive-metasurface-based router. *Nat. Commun.* **2024**, *15*, 2807. [CrossRef]
114. Wagih, M.; Beeby, S. Thin Flexible RF Energy Harvesting Rectenna Surface With a Large Effective Aperture for Sub µW/cm2 Powering of Wireless Sensor Nodes. *IEEE Trans. Microw. Theory Tech.* **2022**, *70*, 4328–4338. [CrossRef]
115. Mansour, M.M.; Takiguchi, O.; Inoi, T.; Kanaya, H. Experimental investigation of wireless energy harvesting with a Bluetooth low energy sensing unit. In Proceedings of the 2018 International Conference on Electronics Packaging and iMAPS All Asia Conference (ICEP-IAAC), Mie, Japan, 17–21 April 2018; pp. 189–193. [CrossRef]
116. Ensworth, J.F.; Reynolds, M.S. BLE-Backscatter: Ultralow-Power IoT Nodes Compatible With Bluetooth 4.0 Low Energy (BLE) Smartphones and Tablets. *IEEE Trans. Microw. Theory Tech.* **2017**, *65*, 3360–3368. [CrossRef]
117. Vera, G.A.; Nawale, S.D.; Duroc, Y.; Tedjini, S. Read Range Enhancement by Harmonic Energy Harvesting in Passive UHF RFID. *IEEE Microw. Wirel. Compon. Lett.* **2015**, *25*, 627–629. [CrossRef]
118. Abdulhadi, A.E.; Abhari, R. Multiport UHF RFID-Tag Antenna for Enhanced Energy Harvesting of Self-Powered Wireless Sensors. *IEEE Trans. Ind. Inform.* **2016**, *12*, 801–808. [CrossRef]
119. Niotaki, K.; Carvalho, N.B.; Georgiadis, A.; Gu, X.; Hemour, S.; Wu, K.; Matos, D.; Belo, D.; Pereira, R.; Figueiredo, R.; et al. RF Energy Harvesting and Wireless Power Transfer for Energy Autonomous Wireless Devices and RFIDs. *IEEE J. Microw.* **2023**, *3*, 763–782. [CrossRef]
120. Lee, W.-K.; Schubert, M.J.W.; Ooi, B.-Y.; Ho, S.J.-Q. Multi-Source Energy Harvesting and Storage for Floating Wireless Sensor Network Nodes With Long Range Communication Capability. *IEEE Trans. Ind. Appl.* **2018**, *54*, 2606–2615. [CrossRef]
121. Cuozzo, G.; Buratti, C.; Verdone, R. A 2.4-GHz LoRa-Based Protocol for Communication and Energy Harvesting on Industry Machines. *IEEE Internet Things J.* **2022**, *9*, 7853–7865. [CrossRef]
122. Mahmoodi, L.; Sadeghi, K.H. Design of Human Passage Detector Based on Simultaneous Wireless Information and Power Transfer Structure. *IEEE Sens. J.* **2025**, *25*, 19532–19544. [CrossRef]
123. Siekkinen, M.; Hiienkari, M.; Nurminen, J.K.; Nieminen, J. How low energy is bluetooth low energy? Comparative measurements with ZigBee/802.15.4. In Proceedings of the 2012 IEEE Wireless Communications and Networking Conference Workshops (WCNCW), Paris, France, 1 April 2012; pp. 232–237. [CrossRef]
124. Lee, J.-S.; Dong, M.-F.; Sun, Y.-H. A preliminary study of low power wireless technologies: ZigBee and Bluetooth Low Energy. In Proceedings of the 2015 IEEE 10th Conference on Industrial Electronics and Applications (ICIEA), Auckland, New Zealand, 15–17 June 2015; pp. 135–139. [CrossRef]
125. Rabeek, S.M.; Raju, S.; Raja, M.K. Design of RF Powered ZigBee Sensor Node and sub 1GHz RF Power Transmitter for Asset Tracking. In Proceedings of the 2021 IEEE Asia-Pacific Microwave Conference (APMC), Brisbane, Australia, 28 November–1 December 2021; pp. 401–403. [CrossRef]
126. Shi, Y.; Fan, Y.; Li, Y.; Yang, L.; Wang, M. An Efficient Broadband Slotted Rectenna for Wireless Power Transfer at LTE Band. *IEEE Trans. Antennas Propag.* **2019**, *67*, 814–822. [CrossRef]
127. Muncuk, U.; Alemdar, K.; Sarode, J.D.; Chowdhury, K.R. Multiband Ambient RF Energy Harvesting Circuit Design for Enabling Batteryless Sensors and IoT. *IEEE Internet Things J.* **2018**, *5*, 2700–2714. [CrossRef]
128. Gu, X.; Grauwin, L.; Dousset, D.; Hemour, S.; Wu, K. Dynamic Ambient RF Energy Density Measurements of Montreal for Battery-Free IoT Sensor Network Planning. *IEEE Internet Things J.* **2021**, *8*, 13209–13221. [CrossRef]

129. Wang, W.; Chen, X.; Liu, Y.; Wang, X.; Liu, Z. Thermo-electric Energy Harvesting Powered IoT System Design and Energy Model Analysis. In Proceedings of the 2019 IEEE 13th International Conference on Anti-counterfeiting, Security, and Identification (ASID), Xiamen, China, 25–27 October 2019; pp. 303–308. [CrossRef]
130. P, S.S.; Tummuru, N.R.; Misra, H. Wireless Power Transfer to Electric Vehicles along with Regenerative Braking using battery-supercapacitor combination. In Proceedings of the 2022 IEEE International Conference on Power Electronics, Smart Grid, and Renewable Energy (PESGRE), Trivandrum, India, 2–5 January 2022; pp. 1–6. [CrossRef]
131. Chew, Z.J.; Ruan, T.; Zhu, M. Strain Energy Harvesting Powered Wireless Sensor System Using Adaptive and Energy-Aware Interface for Enhanced Performance. *IEEE Trans. Ind. Inform.* **2017**, *13*, 3006–3016. [CrossRef]
132. Yang, H.; Li, Y.; Chen, J.; Shao, Y.; Yan, Z.; Mai, R.; He, Z. A Hybrid Load Matching Method for WPT Systems to Maintain High Efficiency Over Wide Load Range. *IEEE Trans. Transp. Electrif.* **2023**, *9*, 1993–2005. [CrossRef]
133. Lin, W.; Ziolkowski, R.W. Wireless Power Transfer (WPT) Enabled IoT Sensors Based on Ultra-Thin Electrically Small Antennas. In Proceedings of the 2021 15th European Conference on Antennas and Propagation (EuCAP), Dusseldorf, Germany, 22–26 March 2021; pp. 1–4. [CrossRef]
134. Kumar, M.; Kumar, S.; Bhadauria, A.S.; Sharma, A. A Planar Integrated Rectenna Array With 3-D-Spherical DC Coverage for Orientation-Tolerant Wireless-Power-Transfer-Enabled IoT Sensor Nodes. *IEEE Trans. Antennas Propag.* **2023**, *71*, 1285–1294. [CrossRef]
135. Yu, B.-Y.; Wang, Z.-H.; Ju, L.; Zhang, C.; Liu, Z.-G.; Tao, L.; Lu, W.-B. Flexible and Wearable Hybrid RF and Solar Energy Harvesting System. *IEEE Trans. Antennas Propag.* **2022**, *70*, 2223–2233. [CrossRef]
136. Abid, A.; O'brien, J.M.; Bensel, T.; Cleveland, C.; Booth, L.; Smith, B.R.; Langer, R.; Traverso, G. Wireless Power Transfer to Millimeter-Sized Gastrointestinal Electronics Validated in a Swine Model. *Sci. Rep.* **2017**, *7*, 46745. [CrossRef]
137. Asif, S.M.; Hansen, J.; Khan, M.S.; Walden, S.D.; Jensen, M.O.; Braaten, B.D.; Ewert, D.L. Design and In Vivo Test of a Batteryless and Fully Wireless Implantable Asynchronous Pacing System. *IEEE Trans. Biomed. Eng.* **2016**, *63*, 1070–1081. [CrossRef]
138. Glaser, P.E. Power from the sun: Its future. *Science* **1968**, *162*, 857–861. [CrossRef]
139. Sasaki, S.; Tanaka, K.; Higuchi, K.; Okuizumi, N.; Kawasaki, S.; Shinohara, N.; Senda, K.; Ishimura, K. A new concept of solar power satellite: Tethered-SPS. *Acta Astronaut.* **2007**, *60*, 153–165. [CrossRef]
140. Dong, S.-W.; Yu, H.; Dong, Y.; Gong, L.; Wang, Y. A new solar power satellite system faced to engineering: Concentric disc. In *2013 IEEE Wireless Power Transfer (WPT)*; IEEE: New York, NY, USA, 2013; pp. 63–65.
141. Sasaki, S.; Tanaka, K. Wireless power transmission technologies for solar power satellite. In Proceedings of the 2011 IEEE MTT-S International Microwave Workshop Series on Innovative Wireless Power Transmission: Technologies, Systems, and Applications, Kyoto, Japan, 12–13 May 2011; pp. 3–6.
142. Liu, C.; He, Z. Investigation on Rectifiers and Rectennas with Various Input Power Levels for the Applications of Space Solar Power Station. *Adv. Astronaut. Sci. Technol.* **2022**, *5*, 39–47. [CrossRef]
143. Dong, Y.; Dong, S.-W.; Gao, S.; Wang, Y.; Li, X.; Wei, G. Design of Microwave Power Transmission System for Space Solar Power Station Demonstration. In Proceedings of the 2020 IEEE Wireless Power Transfer Conference (WPTC), Seoul, Republic of Korea, 15–19 November 2020; pp. 13–15. [CrossRef]